이학박사 학위 논문

의사삼원계의 상거동에 기반한 주름형태 실리카 메조구조체의 형성

Formation of Wrinkled Silica Mesostructures Based on the Phase Behavior of Pseudoternary Systems

2015 년 2 월

서울대학교 대학원

화학부 무기화학전공

문 두 식

Ph. D. Dissertation

Formation of Wrinkled Silica Mesostructures Based on the Phase Behavior of Pseudoternary Systems

Supervisor : Professor Jin-Kyu Lee

Major : Inorganic Chemistry

February 2015

By Moon, Doo-sik

Department of Chemistry

The Graduate School

Seoul National University

Abstract

Formation of Wrinkled Silica Mesostructures Based on the Phase Behavior of Pseudoternary Systems

Moon, Doo-sik

Department of Chemistry, Inorganic Chemistry

The Graduate School

Seoul National University

Recently, mesoporous silica nanoparticles with radial wrinkle structures were introduced almost simultaneously by several groups. Wrinkled silica mesostructures (WSMs) have attracted much attention for their high accessibility to guest materials and large surface area due to those open pore structure. However, the mechanism study about synthesis of these WSMs is not proceeded enough yet. So in this dissertation, the tunable synthetic process of WSMs is investigated to determine the formation mechanism of WSMs.

In Chapter 1, It is explained that the basic research backgrounds about synthesis of mesoporous silica mesostructures and phase behaviors of microemulsion and related systems.

In Chapter 2, the formation mechanism of hierarchical mesoporous silica nanoparticles with wrinkle structure (wrinkled silica nanoparticles, WSNs) was studied and a method for substructure control of silica nanoparticles was proposed. We confirmed that WSNs were generated in the bicontinuous microemulsion phase of the Winsor III system. By using the phase behavior of

Winsor III system, which depends on the water-oil-surfactant mixing ratio, and by adding various cosolvents (cosurfactants), we could precisely control the structure of silica nanoparticles, from the mesoporous to the wrinkle form; furthermore, we could control the inter-wrinkle distance.

In Chapter 3, a profound investigation of water-oil-surfactant ternary systems which have various phase behaviors and substructures that depend on their chemical composition and component ratio is conducted. These substructures can be used as templates for the synthesis of a variety of nanostructures. In this chapter, the phase behavior of a pseudoternary system consisting of aqueous urea–cetyltrimethylammonium bromide (and *n*-butanol)–cyclohexane is analyzed. Additionally, wrinkled silica mesostructures (WSMs) with various morphologies are synthesized using the microemulsion layer in the multi-phase areas of the pseudoternary system with restricted degrees of freedom as a template. The particle size of the wrinkled silica nanoparticles (WSNs) and the connective morphology of the WSMs can be controlled via the catalytic conditions. In addition, some materials which are difficult to produce, such as radially branched WSNs and shuttlecock-shaped Janus nanoparticles, are prepared using a gradual seed-growth mechanism of silica in the emulsion system.

Keywords: Mesoporous, Silica, Nanoparticle, phase behavior, Ternary emulsion system, Winsor systems, Microemulsion

Student Number: 2008-22724

Contents

List of Figures

Chapter 1

Chapter 2

diagram (c) indicates the direction of phase transition when the ratio of oil to water and surfactant is increasing.

Figure 2.2. Scanning electron microscopy (SEM) (upper panel) and transmission electron microscopy (TEM) (lower panel) images of silica nanoparticles synthesized at different heating times.

Figure 2.3. Equilibrium phases of reaction mixtures at different volume ratios of cyclohexane to 15 ml of aqueous solution containing urea (0.3 g), CPB (0.5 g), and *iso*-propanol (0.45 ml).

Figure 2.4. Schematic of separated phases of the Winsor III system, synthesis of silica nanoparticles in each phase, and macroemulsion system (upper panel) and SEM/TEM images of silica nanoparticles from (a and d) upper microemulsion layer, (b and e) lower aqueous layer, and (c and f) macroemulsion system.

Figure 2.5. Schematic (upper panel) and SEM/TEM images (lower panel) of silica nanoparticles synthesized at different volume ratios of cyclohexane to 15 ml of aqueous solution of urea (0.3 g) and CPB (0.5 g) and *iso*-propanol (0.45 ml).

Figure 2.6. Typical 'Kahlweit fish' diagram. The Winsor value R is the variable corresponding to changes in temperature, salinity, and addition of cosolvents. The red/blue arrows indicate phase transitions arisen by the addition of alcohols with short/long alkyl chains.

Figure 2.7. Schematic illustrations of microemulsion phases of reaction mixtures with identical molar amounts of different cosolvents

Figure 3.2. (a–i) SEM images of the silica materials synthesized from the corresponding emulsion systems in Table 3.1.

Figure 3.3. (a) TEM image of mesoporous silica nanoparticles synthesized in the type-IV system. The weight ratio of water (with catalyst):surfactant (with cosurfactant):oil in all reaction mixtures was 7.5:1.0:1.0. (b) SEM image of the silica precipitate synthesized in the type-IV system. The weight ratio of water (with catalyst):surfactant (with cosurfactant):oil in all reaction mixtures is 0.25:1.0:10.0.

Figure 3.4. (a) N_2 adsorption-desorption isotherms and (b) BJH pore-size distribution plots of representative WSMs synthesized in the emulsion systems shown in Table. 3.1.

Figure 3.5. TEM images of the wrinkled silica nanoparticles synthesized with various catalytic systems; (a) Urea 0.4 M + HCl 1 mM, (b) urea 0.4 M + NaOH 1 mM, (c) urea 0.08 M, (d) urea 0.4 M, and (e) urea 2.0 M. The weight ratio of water(with catalyst):surfactant(with cosurfactant):oil in all reaction mixtures was 7.5:1.0:10.0.

Figure 3.6. Changes in the pH values of the water phases of reaction mixtures during heating at 70 °C. The solutions were heated from room temperature to 70 °C and the time at which the temperatures of the solutions reached 70 °C was defined as the zero-point.

Figure 3.7. TEM images of the wrinkled silica nanoparticles synthesized with various catalytic systems: (a) Urea 0.4 M + NaOH 10 mM,

APPENDIX

not applied. (e) Quantitative comparison of signals of each image.

Figure A3. Results of the *In-vivo* bioimaging test. (a) Optical images with fluorescence of rats and collected tissues, (b) fluorescence microscope image of collected tissues.

List of Tables

Chapter 1

Chapter 3

Chapter 1

Research Background

1.1 Mesoporous Silica Materials

Definition and Characteristics of Mesoporous Materials

According to the definition of the International Union of Pure and Applied Chemistry (IUPAC), porous materials are classified into three types depending on the size of the pores which the materials have (Fig 1.1).[1] If a material has pores whose diameter is less than 2 nm, it is microporous, and if the pore diameter is larger than 50 nm, the material is macroporous. And there is a mesoporous material which has pores whose average diameter is 2-50 nm. These materials are utilized in a number of areas according to the respective pore sizes and characteristics. Because the size of the micropores fits monatomic or small molecules appropriately, microporous materials are used for the adsorption or catalysis focused on the small molecules and used in applications such as hydrogen storage, molecular sieve and ion exchange.[2-5] Macroporous materials have a good accessibility due to those large pore size although have small surface area and low selectivity. These are mainly used for an adsorption and separation for materials which have large molecular size.[6,7]

Because of the size of mesopores exceeds the hydrodynamic volume of ordinary molecules, various materials can access those interior easily. Due to those many mesopores, the mesoporous materials have large surface area per unit mass and adequate accessibility. These mesoporous materials can be used

in various areas for example adsorbent, catalyst support, drug delivery and filter.[8-11]

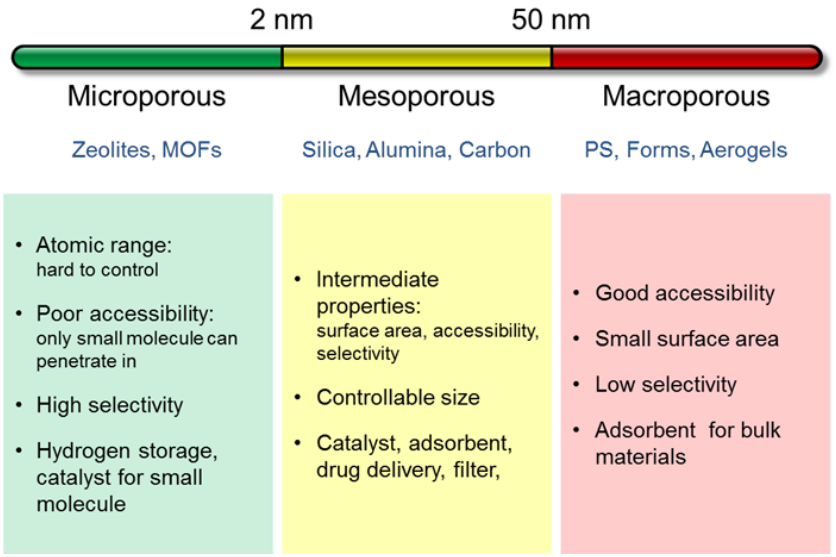

Fig 1.1. Categories of porous materials according to those pore diameter and representative characters of each type.

History and Features of Mesoporous Silica

Since the development of Mobil Crystalline Materials 41 (MCM-41) by Mobil Oil Company in 1992, various mesoporous materials such as Santa Barbara Amorphous type materials (SBA) on the basis of silica were synthesized and utilized with numerous mesostructures and synthetic methods.[12-15]

In 2001, Silica nanoparticles with mesoporous structure were introduced for many application areas need colloidal dispersibility.[16-18] For over a decade,

many researchers synthesized and applied mesoporous silica nanomaterials with various morphologies and pore structures.[19-21]

Since the year 2009, several research groups introduce mesoporous silica nanoparticles with radial wrinkle structure almost same time.[22-26] These have the unique geometrical morphology that those pore width goes wider from inside to outside and each pore is interconnected two-dimensionally. It is expected that these structures have high surface area and good accessibility of guest species, and using these properties, many application studies are in progress.[22,23,27-31]

Synthetic Mechanism of Mesoporous Silica

The synthesis of mesoporous silica is performed using surfactants or copolymers include dendrimers as structure direct agents (SDA). The silica mesostructure is formed on the basis of mesophase made by self-assembly and interaction of SDAs and silicate precursors in aqueous solution.

Meosporous silicas are synthesized via sol-gel process likewise amorphous silicas.[32] In the presence of acid or base catalyst, alkoxysilanes are hydrolyzed and silicates made by the hydrolysis form silica mesostructures by condensation. During this process, charged silicates interact with surfactants which have counter charge and the condensation is performed that the process guided by mesophase of surfactants. There are two typical mechanisms about this process, liquid crystal template mechanism and cooperative self-assembly mechanism (Fig 1.2).[33-35]

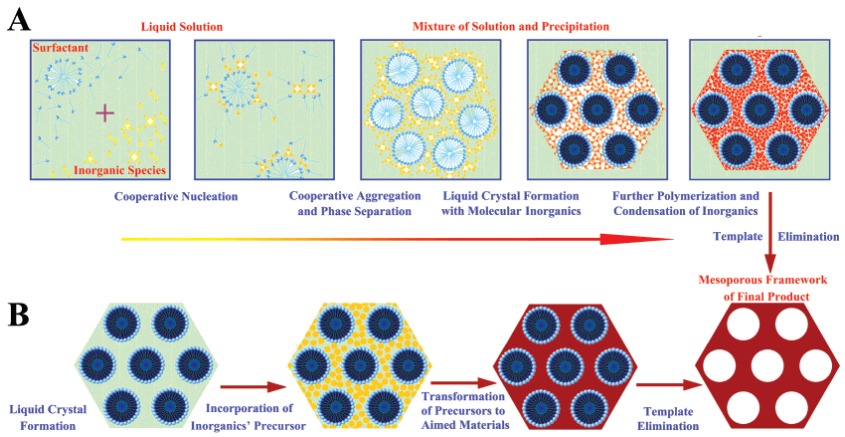

Fig 1.2. Two typical synthetic mechanisms of mesoporous silica. (A) Cooperative self-assembly, (B) liquid-crystal templating process.[35]

The liquid crystal template mechanism is that the mesophase which consist of 2D hexagonal packing structure of 1D channels is formed by self-assembly of surfactants then the mesoporous silica is formed by silicates combine with prepared mesophases (Fig 1.2B).[34] However, this mechanism is not correct for many cases because most reaction conditions have lower concentration of surfactant than minimum concentration that the solution forms liquid crystal phase autonomously. The cooperative self-assembly mechanism was suggested to compliment this problem. It is mechanism that the surfactants and silicates were already interacted and combined before the formation of hexagonal mesophase and the condensation reactions of silicate help the formation of 2D mesophase of silicate-surfactant pairs (Fig 1.2A).[33] In this dissertation, reactions in microemulsion systems will be investigated on the base of this cooperative self-assembly mechanism.

Table 1.1. List of typical mesoporous silica materials

Dimension	Materials	Space group	SDAs	Reference
3D	MCM-41	*p*6*mm*	CTAB	[15]
	FSM-16	*p*6*mm*	CTAB	[36]
	SBA-15	*p*6*mm*	P123 ($EO_{20}PO_{70}EO_{20}$)	[12]
	SBA-3	*p*6*mm*	C_nTMA^+ (n=14~18)	[37]
	SBA-8	*cmm*	CTAB	[38]
	MCM-50	lamellar	CTAB	[39]
2D	MCM-48	$Ia\bar{3}d$	C_nTMA^+ (n=14~18))	[15]
	FDU-12	$Fm\bar{3}m$	F127 ($EO_{106}PO_{70}EO_{106}$)	[43]
	SBA-1	$Pm\bar{3}n$	$C_{16}TEABr$	[37]
	SBA-11	$Pm\bar{3}m$	Brij 56 ($C_{16}EO_{10}$)	[44]
	SBA-16	$Im\bar{3}m$	F127	[44]
Disordered	MSU-1		C_mEO_n (m=11~15)	[45]
	KIT-1		CTACl	[40]
	HMS		$C_mH_{2m+1}NH_2$ (m=8~22)	[41]

Classification of Mesoporous Silica

Mesoporous silica materials can be classified in accordance with structure of those pores (Table 1.1). Above-mentioned MCM-41, SBA-15 and materials such as SBA-3 and FSM-16 have 2D porous structure that 1D channel type mesopores are packed hexagonally. Materials represented by MCM-50 have mesopores with a lamellar structure. MCM-48 is the material whose two types of mesopores are forming 3D cubic structure and there are many other mesoporous silica materials with 3D porous structure with various arrangements (Fig 1.3). And mesoporous silica materials with disordered structures including MSU-X, KIT-1 and HMS were reported. The silica

material with wrinkled structure is one of these disordered mesoporous materials. Mesoporous silica materials can be categorized also by types of structure direct agent used in synthetic process. These are classified into cationic surfactant,[15,36-41] anionic surfactant,[42] nonionic surfactant mainly copolymers.[12,43-45] Because the hydrolyzed silicates are anionic in the most cases, it is hard to synthesis mesoporous silica with normal alkoxysilane and one must add silanes with cationic moiety to the reaction mixture. So this synthetic method with anionic surfactants was introduced relatively lately.

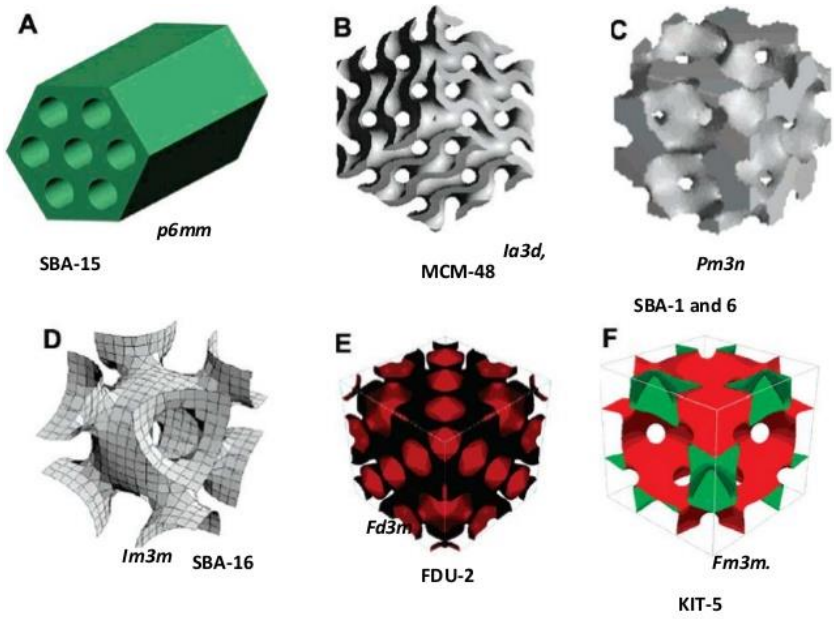

Fig 1.3. Pore models of mesostructures with symmetries of (A) *p*6*mm*, (B) $Ia\bar{3}d$, (C) $Pm\bar{3}n$, (D) $Im\bar{3}m$, (E) $Fd\bar{3}m$, and (F) $Fm\bar{3}m$.[35]

Applications and Prospects of Mesoporous Silica

As above-mentioned, mesoporous silica materials have large surface area and pore volume via those geometrical morphology, chemical stability and easiness of surface modification. So these materials were used in a number of application fields.[21,46-50] The applications as catalytic supports or adsorbents are representative because of those surface area and stability.[46,47] As compared with microporous materials such as zeolites which have pores with monatomic size and have restrictive guest species for use, mesoporous materials have advantage that can use larger molecules such as protein, gene and polymer. In addition, the mesoporous have huge potential of applications such as electrode of lithium battery, water treatment membrane, biosensor, drug delivery and template for synthesis of various nanomaterials.[48-50]

1.2 Emulsions and Related Systems

Definition and Characteristics of Emulsion

The emulsion is subordinate concept of colloid and meaning the colloid whose dispersed phase and continuous phase are both liquid state, in other words, a mixture of two or more immiscible liquids.[51-53] Emulsions are classified into oil-in-water type and water-in-oil according to the phase difference of the mixture of water and hydrophobic solution (in other words, oil). In addition, there are multiple emulsions like water-in-oil-in-water type or oil-in-water-in-oil type depending on the conditions including stirring, composition and temperature. An emulsion whose minor axis is over 100 nm is called the macroemulsion in contrast with the microemulsion which will be discussed in later.[54]

Emulsions stabilize two or more immiscible liquid phases and can be found in numerous places and are utilized in various fields. For example, milk which contains aqueous components and fat species and a lot of foods with cream form makes emulsion phases. Soap and detergent are an application of emulsion. And emulsions are used for drug delivery which makes inject hydrophobic drugs into cells.[51]

Properties of Macroemulsion

Emulsions consist of dispersed phase and continuous phase which are forming interface. Macroemulsions looks cloudy because the incident light is scattered when it meets the interface of the macroemulsions. Because of its

thermodynamic instability, macroemulsions cannot exist spontaneously and must need kinetic forces such as stirring or shaking. If a macroemulsion is leaved without any kinetic forces, it goes back to the stable state via certain processes such as creaming, coalescence, flocculation, and Ostwald ripening.[55] To prevent these phenomena, the surface energy of the interface of the emulsion must be stabilized by addition of surfactants.

Properties of Microemulsion

Microemulsion is transparent (or translucent), isotropic and thermodynamically stable liquid mixture of water, oil, surfactant and occasionally cosurfactant and cosolvent. The range of the minor axis of dispersed phase in the microemulsions is 2 ~ 50 nm, more generally 1 ~ 100.[53,54] Because the distance among the interfaces is under a quarter of the wavelength of visible light, there is scattering of incident light scarcely in the interface of microemulsion and so microemulsion is transparent of translucent. Aqueous phases of microemulsions contain ions or other hydrophilic species usually and oil phases contain lipophilic species. In contrast with macroemulsions which need kinetic forces to maintain interface, microemulsions are thermodynamically stable autonomously and can be formed by simple mixing of those components. There are oil-in-water type and water-in-oil type of the microemulsion likewise the macroemulsion. Also there are microemulsions with bicontinuous substructure.

Phase Behaviors of Ternary Systems

The phase behaviors of water-oil-surfactant ternary systems such as the stabilized state of macroemulsions added surfactants are various and variable.[56-58] If the relative concentration of surfactant is lower than other components' so that the whole range of mixture solution cannot form microemulsion and there is no external kinetic force, the phenomenon that a microemulsion layer which contains most of surfactant in the system separated from one or more extra solvents occurs in equilibrium state. In this case, the amount and types of separated solvents differ according to relative volume (or mass) ratio of emulsion components and affinity of surfactant to water and oil. The affinity of surfactant to water and oil determines internal structure of microemulsions. So we can investigate the internal structure of microemulsions by the comparison of the relative amount of each separated solvent easily without complicated analysis of the microemulsion.[59]

Winsor System

In 1948, P. A. Winsor carried out analysis about trends of above-mentioned ternary systems and the internal structures of each system. And he classified these ternary systems into type I – IV (Fig 1.4).[59-61]

As discussed previously, when the amount of surfactant is insufficient to makes all solvents of the ternary system form microemulsion, a part of solvents form separated microemulsion layer. This microemulsion layer contains the solvent whose affinity to surfactant is higher than other's as

continuous phase of this microemulsion and most of other solvent is expelled from the layer except only small amount which becomes dispersed phase of the microemulsion. For example, if the affinity of surfactant to water is higher sufficiently than affinity to oil, a microemulsion layer is formed that all amount of water phase becomes continuous phase of the microemulsion and a part of oil becomes dispersed phase and other part of oil which separated from the microemulsion became upper layer over microemulsion layer. This type of systems defined as Winsor type I.

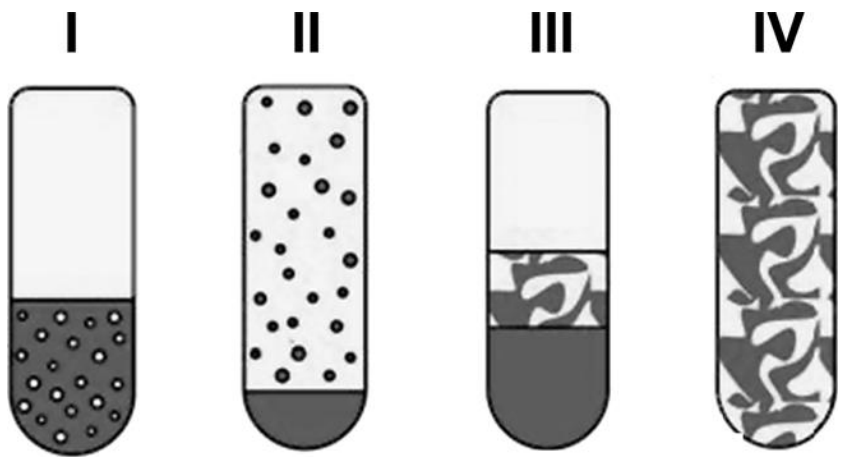

Fig. 1.4. Schematic illustration of the four Winsor systems (light: organic phase, dark: aqueous phase). From left to right: I = (o/w) microemulsion system, II = (w/o) microemulsion system, III = three phase microemulsion system (bicontinuous middle phase), and IV = one phase microemulsion (or bicontinuous system).[62]

On the other hand, if the affinity of surfactant to oil is higher than affinity to water, the microemulsion layer is formed that all amount of oil becomes continuous phase and a part of water becomes dispersed phase and other part

of water is separated and became lower layer under microemulsion layer. This type of systems defined as Winsor type II.

And if the affinity difference is not so big, a part of water and oil become continuous phases interlaced each other and the bicontinuous microemulsion layer is formed. And extra amount of water and oil are separated into lower and upper layer of microemulsion layer respectively. This type of systems defined as Winsor type III.

Finally, if there is a plenty of surfactant, all amount of water and oil can exist in the microemulsion phase independently of relative affinity of surfactant to water and oil. So, there is only one microemulsion phase exist in the total ternary system. This type of systems defined as Winsor type IV, or called as ‘microemulsion’ simply.

The main factor which decides the phase behavior type of ternary systems is basically the affinity and relative concentration of each three components and other factors which affect to the affinity such as temperature, ionic strength, cosolvent and cosurfactant can cause phase behavior transition.

1.3 Scope of the Dissertation

Morphology of mesophase which determine the structure of mesoporous silica is decided by packing parameter of structure directing agents including surfactants and copolymers.[13] To control the porous structures of mesoporous silica materials, one must control the packing parameter of structure directing agents and renew or modify the mesophase. But these systems are too complicated to be calculated analytically and require trials and errors. So most of mesoporous silica materials are hard to control those pore size, and there is a limitation that the range of control is restricted in a dozen nm if possible. And because the most of porous structure of mesoporous silica is capillary tube type, guest materials can stuck at the entrance of mesopores and the efficiency of applications are low actually. To overcome these problem there are copious researches to control size and morphology of mesopores of mesoporous silica materials.[63-65] Several methods using dendrimers of block copolymers or deferent types of surfactant or cosolvent of cosurfactant such as 1,3,5-trimethylbenzene or alcohols have been used to expand or control the porous structure. But the range of pore size control via these methods is still narrow and the method is inconvenient, so the study about synthesis of mesoporous silica with wrinkle structure whose porous structure is easily controllable in wide range is necessary as an alternative.[22,27-30]

However, the mechanism study about synthesis of these silica nanomaterials with radial wrinkled structure is not proceeded enough yet. So

in this dissertation, changing the synthetic conditions in various, the synthetic process of wrinkled silica mesostructures (WSMs) is investigated to determine the formation mechanism of WSMs. And methods to control the inter-wrinkle distance by means of simple change the composition of emulsion or addition of cosolvents (or cosurfactants) are proposed.

The common environment that the WSMs are synthesized is condensation of hydrolyzed silicates in water-oil-surfactant ternary systems discussed in Chapter 1.2. Interactions between silicate and surfactants are investigated in previous synthetic study of mesoporous silica materials, and phase behaviors of water-oil-surfactant ternary systems were researched profoundly throughout the 20th century. But the intimate connection of two research branches for reaction mechanism in the two linked systems has not been accomplished until now. In this dissertation, the mechanism study of the synthesis of WSMs which intimately links two researches is carried out and synthetic methods to form silica materials with various internal-external morphologies is established

1.4 References

[1] Rouquerol, J.; Avnir, D.; Fairbridge, C. W.; Everett, D. H.; Haynes, J. M.; Pernicone, N.; Ramsay, J. D. F.; Sing, K. S. W.; Unger, K. K. In *Pure Appl. Chem.* 1994; Vol. 66, p 1739.

[2] Raja, R.; Thomas, J. M. *J. Mol. Catal. A: Chem.* **2002**, *181*, 3-14.

[3] Schlapbach, L.; Zuttel, A. *Nature* **2001**, *414*, 353-358.

[4] McGarvey, G. B.; Moffat, J. B. *J. Catal.* **1991**, *128*, 69-83.

[5] Bénard, P.; Chahine, R. *Langmuir* **1997**, *13*, 808-813.

[6] Long, C.; Li, A.; Wu, H.; Zhang, Q. *Colloids and Surfaces A: Physicochemical and Engineering Aspects* **2009**, *333*, 150-155.

[7] Svec, F.; Frechet, J. M. J. *Anal. Chem.* **1992**, *64*, 820-822.

[8] Peng, X. S.; Jin, J.; Ichinose, I. *Adv. Funct. Mater.* **2007**, *17*, 1849-1855.

[9] Slowing, I. I.; Trewyn, B. G.; Giri, S.; Lin, V. S. Y. *Adv. Funct. Mater.* **2007**, *17*, 1225-1236.

[10] Vinu, A.; Krithiga, T.; Murugesan, V.; Hartmann, M. *Adv. Mater.* **2004**, *16*, 1817-1821.

[11] Branton, P. J.; Hall, P. G.; Sing, K. S. W.; Reichert, H.; Schuth, F.; Unger, K. K. *J. Chem. Soc., Faraday Trans.* **1994**, *90*, 2965-2967.

[12] Zhao, D.; Feng, J.; Huo, Q.; Melosh, N.; Fredrickson, G. H.; Chmelka, B. F.; Stucky, G. D. *Science* **1998**, *279*, 548-552.

[13] Huo, Q.; Margolese, D. I.; Stucky, G. D. *Chem. Mater.* **1996**, *8*, 1147-1160.

[14] Yang, H.; Kuperman, A.; Coombs, N.; Mamiche-Afara, S.; Ozin, G. A.

Nature **1996**, *379*, 703-705.

[15] Kresge, C. T.; Leonowicz, M. E.; Roth, W. J.; Vartuli, J. C.; Beck, J. S. *Nature* **1992**, *359*, 710-712.

[16] Nooney, R. I.; Thirunavukkarasu, D.; Chen, Y.; Josephs, R.; Ostafin, A. E. *Chem. Mater.* **2002**, *14*, 4721-4728.

[17] Fowler, C. E.; Khushalani, D.; Lebeau, B.; Mann, S. *Adv. Mater.* **2001**, *13*, 649-652.

[18] Cai, Q.; Luo, Z.-S.; Pang, W.-Q.; Fan, Y.-W.; Chen, X.-H.; Cui, F.-Z. *Chem. Mater.* **2001**, *13*, 258-263.

[19] Mihalcik, D. J.; Lin, W. *ChemCatChem* **2009**, *1*, 406-413.

[20] Li, Z.; Barnes, J. C.; Bosoy, A.; Stoddart, J. F.; Zink, J. I. *Chem. Soc. Rev.* **2012**, *41*, 2590-2605.

[21] Trewyn, B. G.; Slowing, I. I.; Giri, S.; Chen, H.-T.; Lin, V. S. Y. *Acc. Chem. Res.* **2007**, *40*, 846-853.

[22] Gai, S.; Yang, P.; Wang, L.; Li, C.; Zhang, M.; Jun, L. *Dalton Transactions* **2012**, *41*, 4511-4516.

[23] Zhang, H.; Li, Z.; Xu, P.; Wu, R.; Jiao, Z. *Chem. Commun.* **2010**, *46*, 6783-6785.

[24] Polshettiwar, V.; Cha, D.; Zhang, X.; Basset, J. M. *Angew. Chem. Int. Ed.* **2010**, *49*, 9652-9656.

[25] Moon, D. S.; Lee, J. K. *Langmuir* **2012**, *28*, 12341-12347.

[26] Pan, W.; Ye, J.; Ning, G.; Lin, Y.; Wang, J. *Mater. Res. Bull.* **2009**, *44*, 280-283.

[27] Du, X.; Shi, B.; Liang, J.; Bi, J.; Dai, S.; Qiao, S. Z. *Adv. Mater.* **2013**, *25*, 5981-5985.

[28] Fihri, A.; Cha, D.; Bouhrara, M.; Almana, N.; Polshettiwar, V. *ChemSusChem* **2012**, *5*, 85-89.

[29] Shen, D.; Yang, J.; Li, X.; Zhou, L.; Zhang, R.; Li, W.; Chen, L.; Wang, R.; Zhang, F.; Zhao, D. *Nano Lett.* **2014**, *14*, 923-932.

[30] Gai, S.; Yang, P.; Ma, P. a.; Wang, D.; Li, C.; Li, X.; Niu, N.; Lin, J. *J. Mater. Chem.* **2011**, *21*, 16420-16426.

[31] Polshettiwar, V.; Thivolle-Cazat, J.; Taoufik, M.; Stoffelbach, F.; Norsic, S.; Basset, J.-M. *Angew. Chem. Int. Ed.* **2011**, *50*, 2747-2751.

[32] Hench, L. L.; West, J. K. *Chem. Rev.* **1990**, *90*, 33-72.

[33] Huo, Q.; Margolese, D. I.; Ciesla, U.; Demuth, D. G.; Feng, P.; Gier, T. E.; Sieger, P.; Firouzi, A.; Chmelka, B. F. *Chem. Mater.* **1994**, *6*, 1176-1191.

[34] Attard, G. S.; Glyde, J. C.; Goltner, C. G. *Nature* **1995**, *378*, 366-368.

[35] Wan, Y.; Zhao *Chem. Rev.* **2007**, *107*, 2821-2860.

[36] Inagaki, S.; Koiwai, A.; Suzuki, N.; Fukushima, Y.; Kuroda, K. *Bull. Chem. Soc. Jpn.* **1996**, *69*, 1449-1457.

[37] Huo, Q.; Margolese, D. I.; Ciesla, U.; Feng, P.; Gier, T. E.; Sieger, P.; Leon, R.; Petroff, P. M.; Schuth, F.; Stucky, G. D. *Nature* **1994**, *368*, 317-321.

[38] Zhao, D.; Huo, Q.; Feng, J.; Kim, J.; Han, Y.; Stucky, G. D. *Chem. Mater.* **1999**, *11*, 2668-2672.

[39] Vartuli, J. C.; Kresge, C. T.; Leonowicz, M. E.; Chu, A. S.; McCullen, S. B.; Johnson, I. D.; Sheppard, E. W. *Chem. Mater.* **1994**, *6*, 2070-2077.

[40] Ryoo, R.; Kim, J. M.; Ko, C. H.; Shin, C. H. *The Journal of Physical Chemistry* **1996**, *100*, 17718-17721.

[41] Tanev, P. T.; Pinnavaia, T. J. *Science* **1995**, *267*, 865-867.

[42] Che, S.; Garcia-Bennett, A. E.; Yokoi, T.; Sakamoto, K.; Kunieda, H.; Terasaki, O.; Tatsumi, T. *Nat Mater* **2003**, *2*, 801-805.

[43] Fan, J.; Yu, C.; Gao, F.; Lei, J.; Tian, B.; Wang, L.; Luo, Q.; Tu, B.; Zhou, W.; Zhao, D. *Angew. Chem. Int. Ed.* **2003**, *42*, 3146-3150.

[44] Zhao, D.; Huo, Q.; Feng, J.; Chmelka, B. F.; Stucky, G. D. *J. Am. Chem. Soc.* **1998**, *120*, 6024-6036.

[45] Bagshaw, S. A.; Prouzet, E.; Pinnavaia, T. J. *Science* **1995**, *269*, 1242-1244.

[46] Maschmeyer, T.; Rey, F.; Sankar, G.; Thomas, J. M. *Nature* **1995**, *378*, 159-162.

[47] Ho, K. Y.; McKay, G.; Yeung, K. L. *Langmuir* **2003**, *19*, 3019-3024.

[48] Luo, J.-y.; Wang, Y.-g.; Xiong, H.-m.; Xia, Y.-y. *Chem. Mater.* **2007**, *19*, 4791-4795.

[49] Sayari, A.; Hamoudi, S.; Yang, Y. *Chem. Mater.* **2005**, *17*, 212-216.

[50] Kim, J.; Kim, H. S.; Lee, N.; Kim, T.; Kim, H.; Yu, T.; Song, I. C.; Moon, W. K.; Hyeon, T. *Angew. Chem. Int. Ed.* **2008**, *47*, 8438-8441.

[51] Israelachvili, J. *Colloids and Surfaces A: Physicochemical and Engineering Aspects* **1994**, *91*, 1-8.

[52] Everett, D. H. In *Pure Appl. Chem.* 1972; Vol. 31, p 577.

[53] Slomkowski, S.; Alemán José, V.; Gilbert Robert, G.; Hess, M.; Horie, K.; Jones Richard, G.; Kubisa, P.; Meisel, I.; Mormann, W.; Penczek, S.; Stepto Robert, F. T. In *Pure Appl. Chem.* 2011; Vol. 83, p 2229.

[54] Olsson, U.; Lindman, B. *Colloids and Surfaces A: Physicochemical and Engineering Aspects* **1997**, *123*, 13-26.

[55] Borwankar, R. P.; Lobo, L. A.; Wasan, D. T. *Colloids and surfaces* **1992**, *69*, 135-146.

[56] Kahlweit, M.; Strey, R.; Firman, P.; Haase, D. *Langmuir* **1985**, *1*, 281-288.

[57] Shinoda, K.; Saito, H. *J. Colloid Interface Sci.* **1968**, *26*, 70-74.

[58] Jada, A.; Lang, J.; Zana, R. *J. Phys. Chem.* **1990**, *94*, 381-387.

[59] Winsor, P. A. *Chem. Rev.* **1968**, *68*, 1-40.

[60] Winsor, P. *Transactions of the Faraday Society* **1948**, *44*, 376-398.

[61] Binks, B. *Langmuir* **1993**, *9*, 25-28.

[62] Schwarze, M.; Pogrzeba, T.; Volovych, I.; Schomacker, R. *Catalysis Science & Technology* **2015**, *Online-Published*.

[63] Widenmeyer, M.; Anwander, R. *Chem. Mater.* **2002**, *14*, 1827-1831.

[64] Kim, M. J.; Ryoo, R. *Chem. Mater.* **1999**, *11*, 487-491.

[65] Zhao, D.; Sun, J.; Li, Q.; Stucky, G. D. *Chem. Mater.* **2000**, *12*, 275-279.

Chapter 2

Tunable Synthesis of Hierarchical Mesoporous Silica Nanoparticles with Radial Wrinkle Structure

2.1 Introduction

Silica nanoparticles have been used in various applications such as catalysis, drug delivery, gene therapy, and biosensor mechanism, due to simple synthetic process, chemical stability, ease of surface modification, and relatively low cytotoxicity.[1-6] Since the synthesis of MCM-41 by the Mobil oil company,[7] several research groups have focused on mesoporous silica, and several advancements have been made in this direction. Because of its very large surface area and pore volume, mesoporous silica has been utilized in wide-ranging applications involving adsorption, separation, and the creation of a hard template for the substructure of other materials.[8-15] In addition, there have been many studies focusing on the synthesis and application of spherical mesoporous silica nanoparticles for in-vivo usage, packing materials in chromatography, quasi-homogeneous catalysts, etc.[16-20] However, it is hard to control the pore size of mesoporous silica materials, and control is only possible within the range of several nanometers.[21] Furthermore, in actual applications with mesopores having capillary tube shapes, the poor accessibility of functional materials inside pores generally cause complications. Despite several studies that examine the morphology

control of mesoporous silica in order to address the abovementioned issues, the ability to control the silica structure and range of pore size is still very limited.[20,22-27]

Very recently, spherical silica nanoparticles with radial wrinkle structure (wrinkled silica nanoparticles, WSNs) have been newly synthesized, and they have been studied for use in support materials for drug delivery and catalysis.[28-31] Their small size in nanometer range and large surface-to-volume ratio allows their dispersion in various solvents as a colloidal solution, and their radial wrinkle structure which widens radially outward is expected to enhance the accessibility of functional materials inside their pores. However, there has been a lack of sufficient research towards understanding the formation mechanism of WSNs. Moreover, in contrast to the opinion that the wrinkle structure is formed from the water-in-oil reverse micelle basis,[30] the composition of the reaction mixture seems to be closer to the oil-in-water emulsion phase. Therefore, an understanding of the formation mechanism and the precise control of particle sizes and radial wrinkle structures is of considerable interest.

Several research results since the early 1900s have reported on properties of ternary systems of water, oil, and surfactants.[32-34] In particular, Winsor performed a systematic classification of structures and behaviors of the emulsion phases at low surfactant concentrations.[35] The ternary systems of polar solvents (represented by water), nonpolar solvents (oil), and surfactants show 4 types of phase behavior (the so-called ‘Winsor system’). This

behavior is determined by surfactant concentration and the Winsor value R which is a variable depending on temperature, salinity, and affinity of each component. When the concentration of the surfactant relative to that of water and oil, is sufficiently high (but lower than the concentration at which mesophases, such as the lamella phase, are formed), the system is said to be a Winsor IV system, in which the three components of the mixture form only one microemulsion phase. If the amount of surfactant is small when compared with those of the two immiscible solvents, mixtures form Winsor I-III systems, in which an excess amount of solvent is separated from the microemulsion of the water-oil-surfactant ternary system, and an independent phase is formed (Fig. 2.1).[35-37]

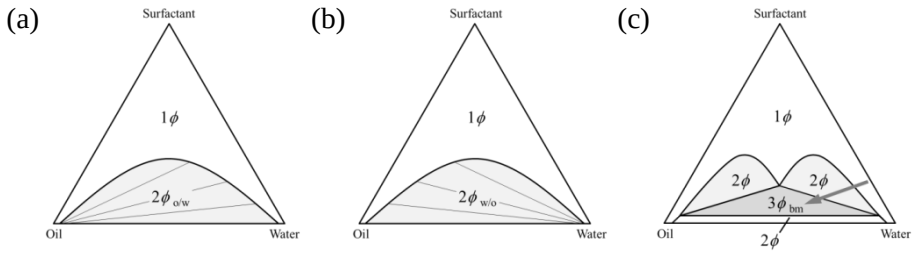

Figure 2.1. Typical phase behaviors of Winsor systems: (a) type I, (b) type II, and (c) type III. The term 'nϕ's indicates the number of phases, and subscripts indicate the structure of the emulsion phases contained in each system. (o/w: oil-in-water, w/o: water-in-oil, bm: bicontinuous microemulsion) The gray arrow in the diagram (c) indicates the direction of phase transition when the ratio of oil to water and surfactant is increasing.

When the Winsor value R is less than 1, the mixtures form a Winsor I system; this is the biphasic system with the oil-in-water microemulsion layer and an extra oil layer. For R > 1, the system forms a Winsor II system, and it constitutes a water-in-oil microemulsion layer and an extra water layer. In particular, for a specific affinity value of the three components and at a certain temperature (R is close to 1), the mixture forms the Winsor III system that contains a bicontinuous microemulsion phase consisting of most of the surfactant along with similar amounts of water and oil in the middle layer of the mixture. The excess water and oil are separated into the bottom and top layers of the microemulsion layer (it is noteworthy that three phases can exist when appropriate amounts of water, oil, and surfactant are mixed while maintaining the Winsor value R at approximately 1).

In this study, to understand the mechanism underlying the formation of silica nanoparticles with radial wrinkle structures, we investigated the hierarchical structures of silica nanoparticles generated from various reaction conditions, and we confirmed that the phase of the reaction mixtures in these cases correspond to the Winsor III system. Based on the result that unique hierarchical structures are formed from the emulsion phase behavior of the reaction mixture, we suggest a simple and easy method to control the structure of silica nanoparticles.

2.2 Experimental Section

Chemicals and Instrumentation

Cetylpyridinium bromide (CPB) was purchased from Aldrich and triethylorhtosilicate (TEOS) was purchased from TCI. Urea, cyclohexane, toluene, *iso*-propanol, *n*-butanol, and *n*-pentanol, were purchased from Samchun Chemical. All the chemicals were used as received without further purification. Scanning electron microscopy (SEM) and transmission electron microscopy (TEM) were conducted using Hitachi H-4300 (Hitachi) and Hitachi H-7600 (Hitachi), respectively. Nitrogen adsorption-desorption isotherms and pore size distributions were measured using Micromeritics ASAP 2020 (Micromeritics).

Synthesis of Mesoporous Silica Nanoparticles with Radial Wrinkle Structure

Silica mesoporous nanoparticles with radial wrinkle structure were prepared by modifying the procedure reported in the literature.[28,30] As a representative example, the typical synthetic conditions are as follows. Firstly, 0.5 g (1.3 mmol) of cetylpyridinium bromide and 0.3 g (5.0 mmol) of urea were dissolved in 15 ml of water. Subsequently, 15 ml of cyclohexane and 0.46 ml (6 mmol) of *iso*-propanol were added to the solution. With vigorous stirring, 1.25 g (6 mmol) of TEOS was added dropwise to the mixed solution. After vigorous stirring for 30 min at room temperature, the reaction mixture was heated up to 70 ℃, and this state was maintained for 16 h. The reaction

mixture was centrifuged and washed with acetone and water thrice, and subsequently, the mixture was redispersed in 50 ml of ethanol. To remove the surfactant from the silica nanoparticles, 4 ml of 12 M hydrochloric acid was added, and the solution was stirred for 24 h at 70 ℃. In other cases, various structures of silica nanoparticles were synthesized under specific conditions by varying several factors, such as reaction time, volume ratio of solvents, a type of organic solvents or cosolvents.

2.3 Results and Discussion

Monitoring the Generated Structures at Various Heating Times

After vigorous stirring for 30 min at room temperature, the reaction mixture was heated at 70 ℃; a typical synthetic condition included cetylpyridinium bromide (CPB; 0.5 g, 1.3 mmol), urea (0.3 g, 5.0 mmol), and TEOS (1.25 g, 6.0 mmol) in the mixed solvents of water (15 ml), cyclohexane (15 ml), and *iso*-propanol (0.46 ml, 6.0 mmol). After certain periods of heating time, small portions of the reaction mixture were collected and the products were isolated to be characterized by SEM and TEM. The amount of nanoparticles obtained by centrifugation was insufficient to be separated from the reaction mixture in order to be used for characterization before 8 h of heating. After 8 h of heating, at an early reaction stage, nanoparticles with diameters of 50~200 nm (average diameter: 156 ± 39 nm) were formed; however, the amount of isolated silica nanoparticles was still small. The size and amount of nanoparticles increased (average diameter: 197 ± 30 nm, 222 ± 27 nm, 282 ± 20 nm at 10 h, 12 h, and 16 h, respectively) with increasing heating time. Interestingly, upon comparing nanoparticles obtained at an early reaction stage with sufficiently grown nanoparticles obtained at later reaction stages, it was found that the average inter-wrinkle distances were almost identical and independent of the sizes of nanoparticles (Fig. 2.2). From these results, we speculated that silica nanoparticles could be grown via a bicontinuous template with a fixed average distance between its layers under typical reaction conditions.[31]

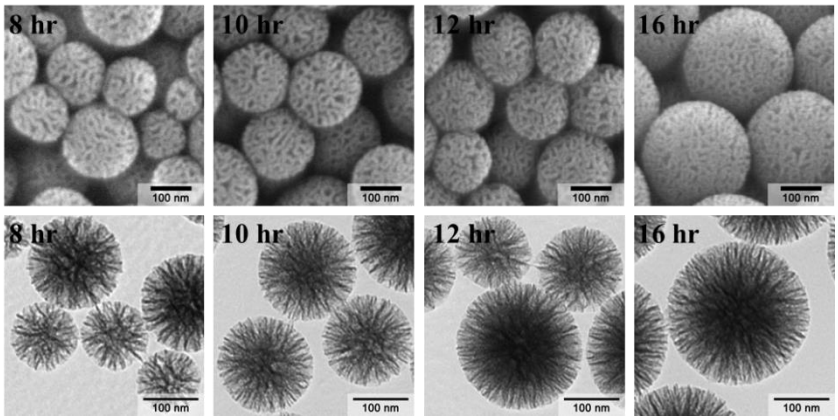

Figure 2.2. Scanning electron microscopy (SEM) (upper panel) and transmission electron microscopy (TEM) (lower panel) images of silica nanoparticles synthesized at different heating times.

Winsor III System

In the Winsor III system, when the amount of oil gradually increase from a mono-phase (1ϕ) system (direct micelle phase) comprising water and surfactant, the system becomes a three-phase (3ϕ) system while transitioning through a two-phase system (2ϕ), and this three-phase system contains a water-rich microemulsion layer and an extra water layer (as indicated by the arrow in Fig. 2.1c). While the amount of oil increases, the Winsor value R should be maintained to approximately 1 in order to maintain the Winsor III system. However, this R value is not clearly defined and rationally predictable value; instead, it is a very broad complex term depending on the temperature, salinity, and affinity of each component in the mixture. Therefore, the easiest and simplest way to check whether the mixed system belongs to the Winsor

III type is to obtain actual samples and observe the formation of the three phases at the equilibrium state.

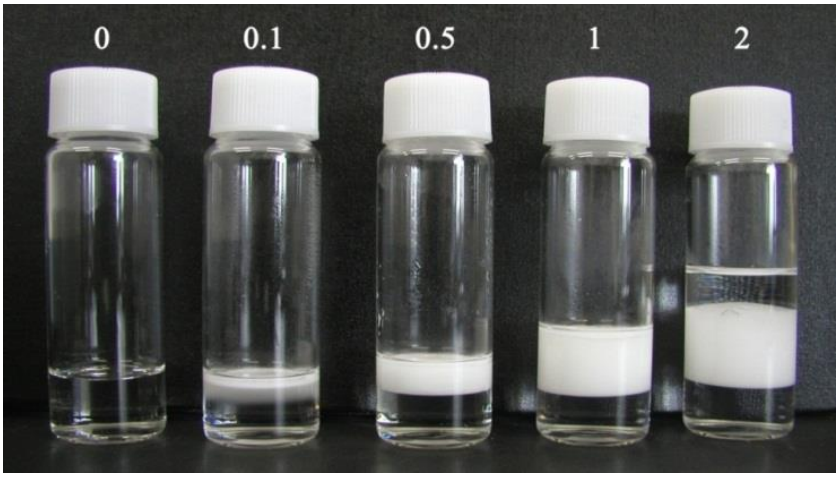

Figure 2.3. Equilibrium phases of reaction mixtures at different volume ratios of cyclohexane to 15 ml of aqueous solution containing urea (0.3 g), CPB (0.5 g), and *iso*-propanol (0.45 ml).

Figure 2.3 shows images of equilibrium phases that were generated from mixed solutions of cyclohexane and aqueous solution containing urea, CPB, and *iso*-propanol with different volume ratios. When the volume ratio of cyclohexane to the aqueous solution was increased to 1, two distinct phases could be observed. The upper layer of cyclohexane could be clearly observed when the ratio was further increased to 2, thereby confirming that the mixed system was in the Winsor III system region. The middle layer of this system should ideally comprise a bicontinuous microemulsion structure. Figure 2.1c shows a typical phase diagram of the Winsor III system in which the microemulsion structure of the two-phase region from the mixture with the

smaller cyclohexane volume ratio (0.1, 0.5, and 1) is an intermediate microemulsion between oil-in-water micellar and bicontinuous structures.

The upper microemulsion and the lower aqueous phase of the system with a 1:1 volume ratio of cyclohexane to aqueous mixture (Fig. 2.3) were separated and 0.8 ml of TEOS was added to each part. Both mixtures were made to separately react with the TEOS solution for 24 h at 70 ℃. As a result, mesoporous silica nanoparticles with pore sizes of 2~3 nm were generated from the lower layer (Figs. 2.4b and e) while silica nanoparticles with wrinkle structures were obtained from the upper layer (Figs. 2.4a and d). From these results, we were able to confirm that the bicontinuous microemulsion phase of the Winsor III system is essential to the formation of the wrinkle structure of silica nanoparticles. However, silica nanoparticles synthesized from the bicontinuous phase of the separated upper layer were aggregated, and these nanoparticles showed a wider particle size distribution when compared with those from the macroemulsion system obtained by the fast mechanical stirring of the two separated layers (Figs. 2.4c and f). When aliquots of this macroemulsion system were added to pure water or cyclohexane, they diluted quickly in water but stayed in a separated droplet shape in cyclohexane, thereby confirming that this macroemulsion system is an oil-in-water type emulsion within which the bicontinuous microemulsion is dispersed, as schematically shown in Figure 2.4. This macroemulsion system allows the synthesis of well-separated silica nanoparticles by continuous hydrolysis and

condensation of TEOS with a monodisperse size distribution when compared with those obtained from the creamed microemulsion phase.

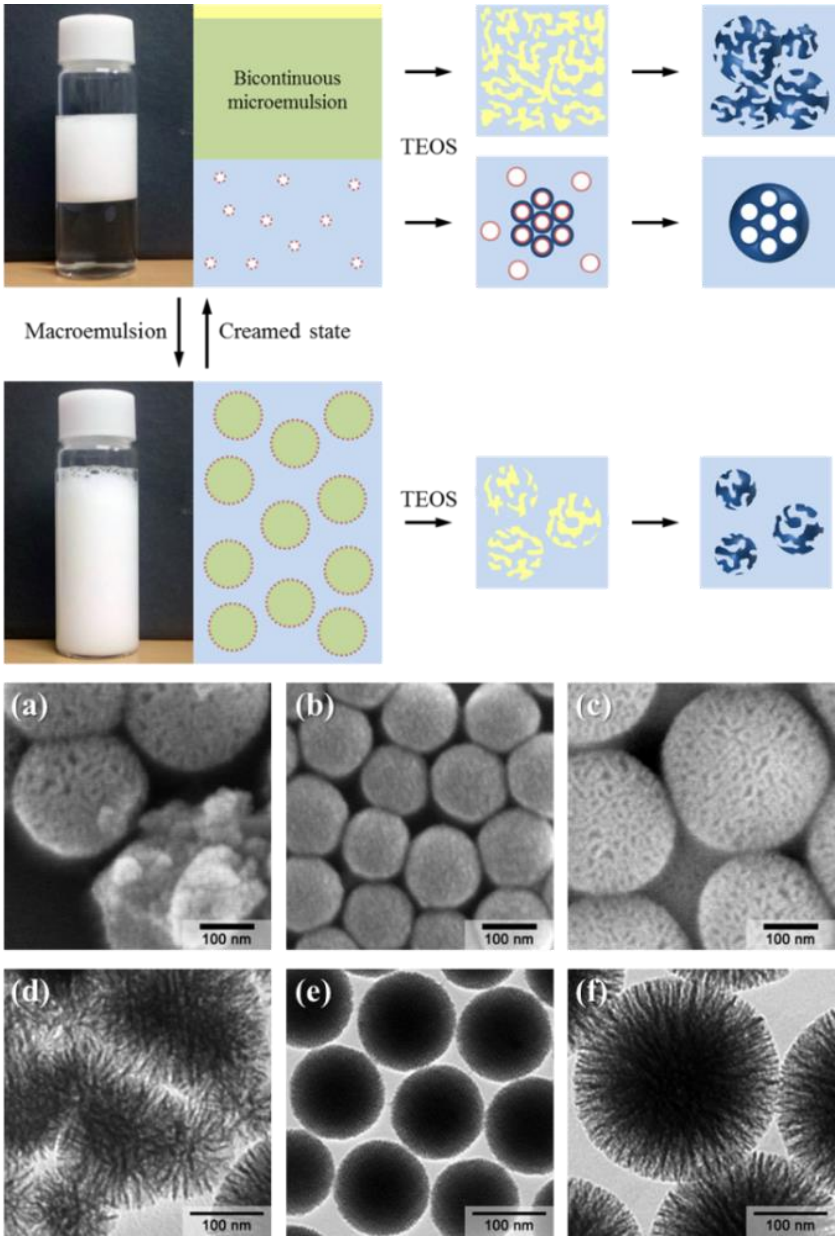

Figure 2.4. Schematic of separated phases of the Winsor III system, synthesis of silica nanoparticles in each phase, and macroemulsion system (upper panel) and SEM/TEM images of silica nanoparticles from (a and d) upper microemulsion layer, (b and e) lower aqueous layer, and (c and f) macroemulsion system.

Morphology Changes of Silica Nanoparticles as a Function of the Volume Ratio of Cyclohexane to Aqueous Solution

Based on the typical phase diagram of the Winsor III system (Fig. 2.1c), when additional oil is gradually added with fixed amount of water and surfactant (sometimes including cosolvent) within a specific reaction condition region, the equilibrium state of the mixture changes from monophasic to biphasic, and further to triphasic system. The emulsion structure within the microemulsion layer also changes from direct micelle to oil-in-water swollen micelle, and finally to a bicontinuous microemulsion structure.[36,38] When TEOS was added to mixtures comprising various volume ratios of cyclohexane and an aqueous solution of CPB, urea, and *iso*-propanol, different microemulsion structures were obtained; therefore, various microemulsion structures and morphologies of silica can be obtained with this method. When TEOS was used to predetermine the microemulsion structures of the various mixtures with different volume ratios (ranging from 0 to 1) of cyclohexane to aqueous solution, it was observed that the resulting silica nanoparticles structure varied from very tight mesoporous to expanded mesoporous, mixed (or broken) mesoporous, and finally, the wrinkled structure (Fig. 2.5). This trend of morphology changes corresponds to the phase behavior of the Winsor III system, and this trend can further support the previously suggested synthetic mechanism underlying the formation of silica nanoparticles with radial wrinkle structures based on the Winsor III system.

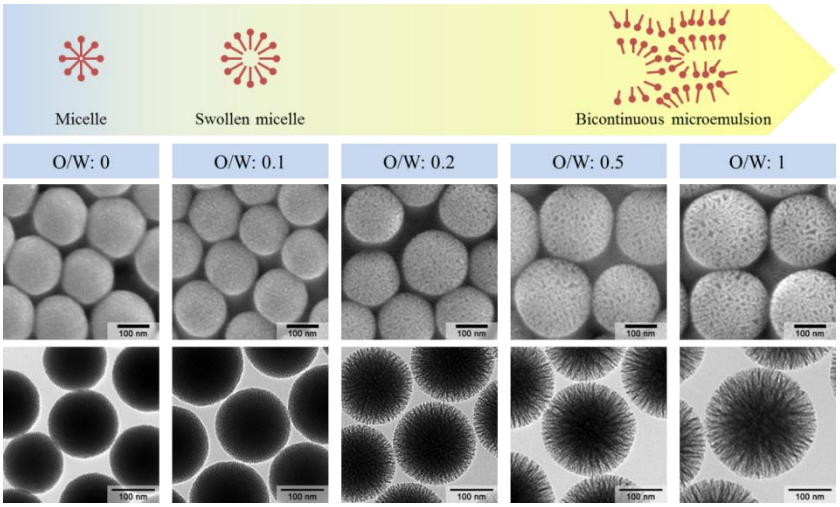

Figure 2.5. Schematic (upper panel) and SEM/TEM images (lower panel) of silica nanoparticles synthesized at different volume ratios of cyclohexane to 15 ml of aqueous solution of urea (0.3 g) and CPB (0.5 g) and *iso*-propanol (0.45 ml).

Effects of Cosolvents on Morphologies of Silica Nanoparticles

In general, Winsor I, II, and III systems follow a phase diagram (the so-called 'Kalweit fish' diagram), and transitions occur among the three systems due to variations in temperature, surfactant concentration, salinity, and the type and the amount of additional cosolvents (Fig. 2.6).[38-40] In particular, the addition of cosolvents (usually alkyl alcohols) alters phase behavior by changing the relative solubility of the surfactants in water and oil. Alcohols with short alkyl chains show good miscibility with water; these alcohols lower the hydrophobicity of surfactants and enhance the interaction between the excess water and the microemulsion phase when they are added to an emulsion system. Consequently, the microemulsion structure is closer

identified with the oil-in-water form and the phase behavior changes from the Winsor III to the Winsor I system (in the direction indicated by the red arrow in Fig. 2.6), thereby leading to an increase in the volume fraction of water in the emulsion phase. In contrast, alcohols with long alkyl chains raise the hydrophobicity of surfactants; as a result, the transition of phase behavior from the Winsor III to the Winsor II system occurs and the volume fraction of the oil layer in the emulsion phase increases (this behavior direction is indicated by the blue arrow in Fig. 2.6).[38]

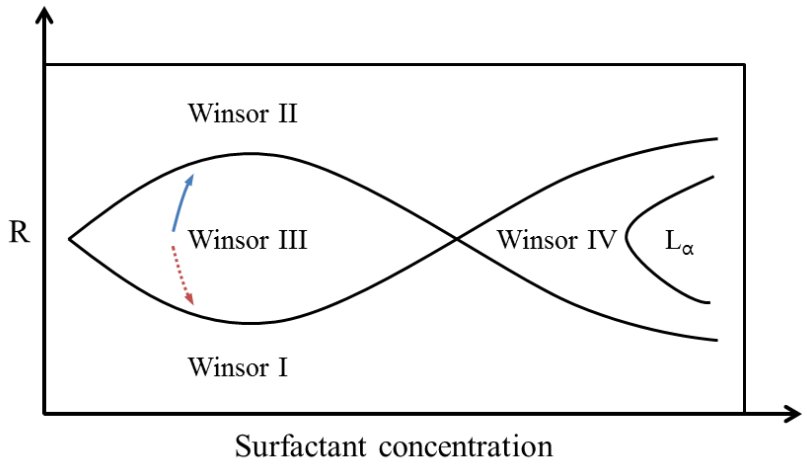

Figure 2.6. Typical 'Kahlweit fish' diagram. The Winsor value R is the variable corresponding to changes in temperature, salinity, and addition of cosolvents. The red/blue arrows indicate phase transitions arisen by the addition of alcohols with short/long alkyl chains.

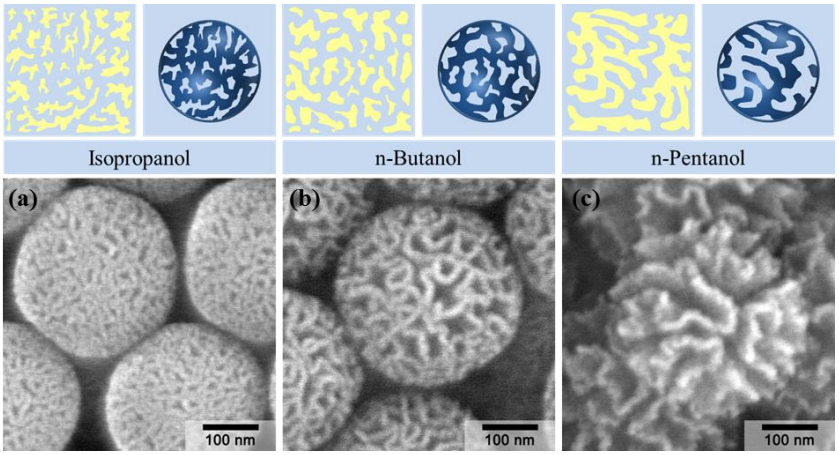

Figure 2.7. Schematic illustrations of microemulsion phases of reaction mixtures with identical molar amounts of different cosolvents and SEM images of WSNs generated from these mixtures. (a) 0.46 ml (6.0 mmol) of *iso*-propanol, (b) 0.55 ml (6.0 mmol) of *n*-butanol, (c) 0.65 ml (6.0 mmol) of *n*-pentanol.

In our study, similar trends were observed in the synthesis of silica nanoparticles with wrinkle structures. Upon increasing the chain length of cosolvents that were added to the mixtures with an identical mixing ratio, it was found that the inter-wrinkle distances in silica nanoparticles increased (Fig. 2.7). Because these changes in inter-wrinkle distance were influenced by the affinity between oil and the surfactant of the emulsion phase, the hydrophobicity of oils could influence the inter-wrinkle distance in a manner similar to that by the cosolvents. To confirm this speculation, we used toluene as the oil phase (toluene has higher polarity than cyclohexane), and *iso*-propanol and *n*-butanol were added to each mixture as cosolvents for the synthesis of silica nanoparticles. As expected, generated wrinkle structures

showed a wider separation between each wrinkles as compared with those obtained using cyclohexane as the oil phase even though identical types and the amount of cosolvents were used (Fig. 2.8). However, no regular nanoparticles were formed when *n*-pentanol was used as a cosolvent. Based on the tendency of the inter-wrinkle distance, in this case, the transition of the emulsion phase appears to occur within the bicontinuous region. We speculate that the water-in-oil phase region, which has no continuous aqueous layer, may block the reaction, thereby preventing the formation of nanoparticles. Further, the Winsor value R may have significantly changed, thereby changing the conditions required for the mixture to remain as a Winsor III system, when toluene and *n*-pentanol were employed as oil and cosolvent; no further experiments were carried out to study these details.

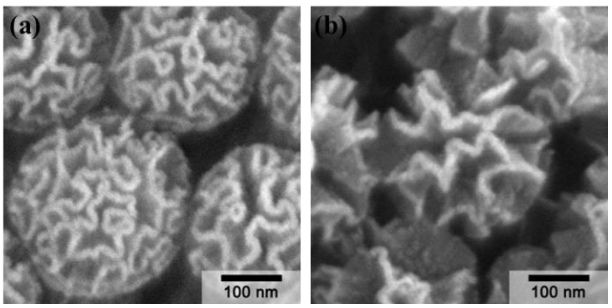

Figure 2.8. SEM images of WSNs synthesized using 15 ml of toluene as oil phase and (a) 0.46 ml (6.0 mmol) of *iso*-propanol, (b) 0.55 ml (6.0 mmol) of *n*-butanol were added as cosolvents.

Hierarchical Mesoporous Structure on Wrinkles

Brunauer, Emmett, Teller (BET) surface areas of WSNs synthesized with different cosolvents (*iso*-propanol, *n*-butanol, and *n*-pentanol) measured by N_2 adsorption-desorption isotherms were 520.3, 573.2, and 592.7 m^2/g respectively. Shapes of N_2 adsorption-desorption isotherms of these nanoparticles were slightly different from a typical type IV which has only one step in the middle range of relative pressure (P/P_0). Those additional large N_2 uptakes and H_3 hysteresis at the relative pressure near 1.0 have been explained as there are large amount of macro pores with a slit shapes. Except for the case when *n*-pentanol was used as a cosolvent, we can see that pore size distributions consist of sharp peaks in the 2~4 nm range and wide bands in the 15~50 nm range; when longer alkyl alcohols were used, wider and lower bands were formed (Fig. 2.9).

Upon comparing these results with the SEM images shown in Figure 2.5, it appears that these wide bands in the 15~50 nm range correspond to inter-wrinkle distances. In the case of the nanoparticles formed with *n*-pentanol, obtained wrinkles show too large a distance between them and too open a shape to be detected as mesopores by N_2 adsorption-desorption because no condensation of N_2 gas occurred on the particle surface. Sharp peaks in the 2~4 nm range that appear in every plot suggest that these particles have a mesoporous structure besides wrinkles, i.e., each wrinkle forming nanoparticles is a membrane with a mesoporous structure.

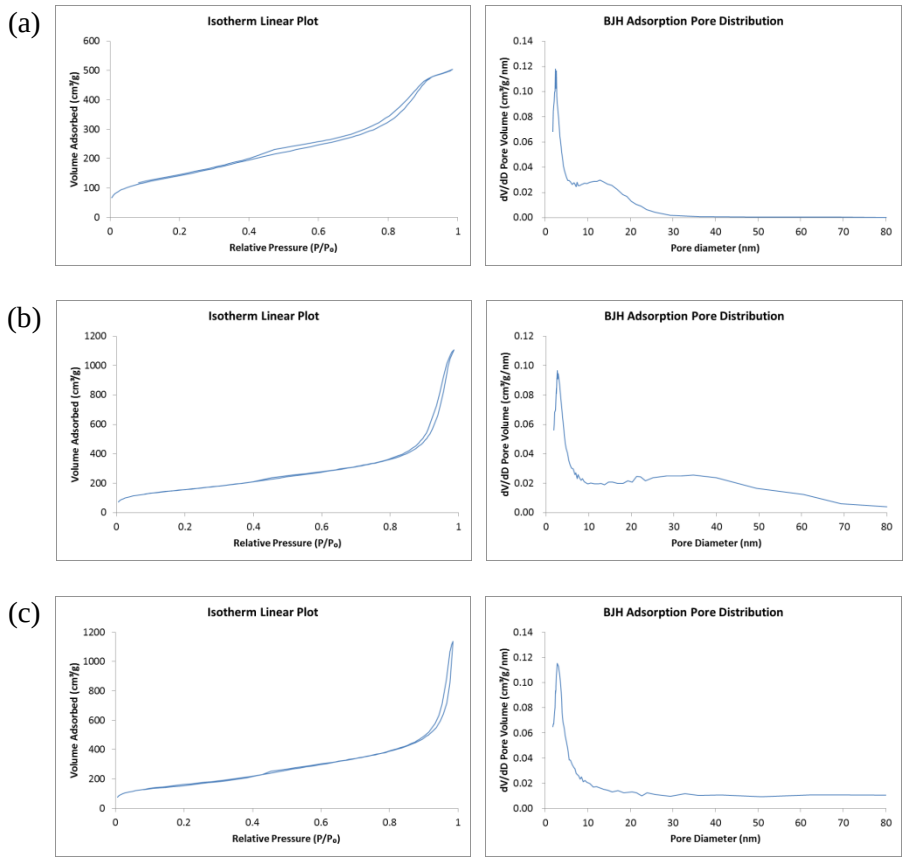

Figure 2.9. N_2 adsorption-desorption isotherms and pore size distribution plots of WSNs synthesized using 15 ml of cyclohexane as oil phase and (a) 0.46 ml (6.0 mmol) of *iso*-propanol, (b) 0.55 ml (6.0 mmol) of *n*-butanol, and (c) 0.65 ml (6.0 mmol) of *n*-pentanol were added as cosolvents.

On the basis of previously reported synthetic mechanisms of mesoporous silica nanoparticles and microemulsion phase behaviors of corresponding reaction mixtures, we speculate as to how the hierarchical mesoporous structure on the WSNs is produced. As reported in the literature,[41] TEOS dissolved in the oil layer comes into contact with the water at the emulsion interface, and hydrolysis and condensation reactions occur.[37] In the basic

solution, the reaction mixture contains ionized silicate monomers and oligomers that have negative charges; these silicates can bind to head-groups of cationic surfactants by the Coulomb interaction. As the condensation reaction proceeds, the amount of partially condensed (~Q^3) silicates decreases and that of fully condensed (Q^4) silicates increases. These Q^4 silicates cannot be ionized; consequently, the total negative charge density of silicates decreases. In order to maintain charge balance, the number of silicate attached to a head-group of surfactant with multidentate binding increases, and consequently, the head-group area of the surfactant increases. Accordingly, the curvature of the water-oil interface surrounded by surfactants increases to the positive direction and this interface can form closed structure such as spherical or cylindrical shapes.[41] This process coincides with the percolation theories of an emulsion film rupture and an emulsion inversion occurs at the phase inversion temperature.[42,43] These surfactant-silicate systems with closed structure can be demulsified from the emulsion phase, and micelles or micellar emulsions are formed. The aggregation of these micelles leads to the formation of a repetitive mesophase (Fig. 2.10). This mesophase probably acts as a nanoparticle seeding site and nanoparticles grow through the water layer of bicontinuous microemulsion phase in the reaction system we have discussed. As nanoparticles start growing, the structure of microemulsion around each nanoparticle is rearranged; water layers of the microemulsion are connected with the ridges of nanoparticle wrinkles and oil layers of the microemulsion are connected with the valleys of nanoparticle wrinkles.

Through water layers that are connected with ridges, newly formed mesophases are deposited on nanoparticle seeds, and the overall structure of nanoparticle assumes the wrinkle shape. Finally, a hierarchical mesoporous structure is formed on the wrinkles.

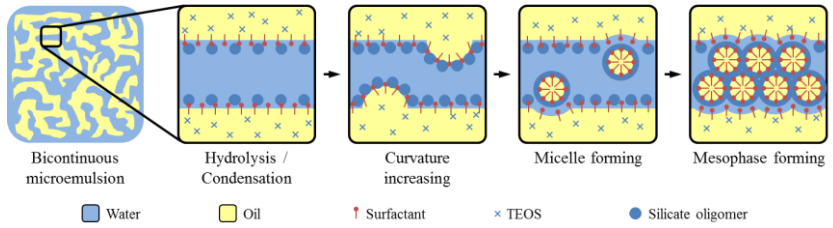

Figure 2.10. Schematic illustration of the mesophase forming mechanism from the microemulsion interface.

In this process, the urea carries out a role as a base catalyst for hydrolysis and condensation of silicates by thermal decomposition.[28] At the starting point of the reaction, the reaction mixture was nearly neutral (pH 7), and as the reaction proceed at 70 ℃, Its pH was increased continuously to about 10. It seems that the continuous pH change of the reaction mixture controls the reaction rate adequately to make nanoparticles in spherical shape. When ammonium hydroxide was directly added as a base catalyst, the distinguished wrinkle structure of WSNs could be observed but the overall shape of particles was very irregular (Fig. 2.11).

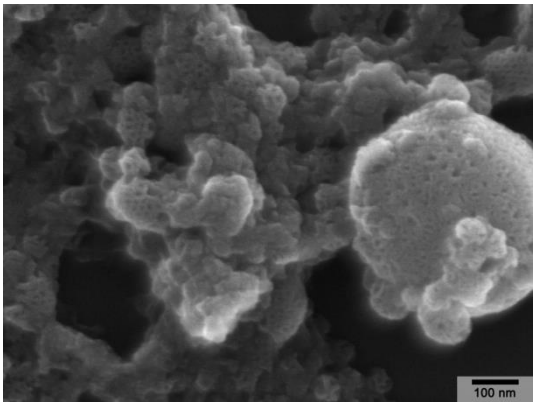

Figure 2.11. SEM image of WSNs synthesized using $NH_4OH_{(aq)}$ as a base catalyst. 0.3 ml of 28% $NH_4OH_{(aq)}$ was added to the typical synthetic condition instead of urea.

2.4 Conclusion

We confirmed that the reaction mixture of cyclohexane and aqueous solution containing urea, CPB, and alcohol at a specific ratio could form the Winsor III system. Further, we showed that hierarchical mesoporous silica nanoparticles with a radial wrinkle structure were produced in the bicontinuous microemulsion phase. By deliberately controlling the microemulsion phase behavior, based on the effect of additional alcohols having different alkyl chain length as cosolvents, we were able to precisely tune inter-wrinkle distances of wrinkled silica nanoparticles (WSNs).

In addition, we showed that wrinkles in nanoparticles exhibited hierarchical mesoporous structures by means of N_2 adsorption-desorption analysis. This formation can be explained by theories of mesoporous silica formation and emulsion rupture-inversion.

We believe that this new tunable synthetic method of hierarchical mesoporous WSNs can be used in various applications, such as catalyst support, drug delivery with controllable release times, selective adsorption of proteins or DNA on the basis of molecular size, special packing to control the speed of moving fluid, and templates for other materials to form substructure.

2.5 References

[1] Minakata, S.; Komatsu, M. *Chem. Rev.* **2008**, *109*, 711-724.

[2] Burns, A.; Ow, H.; Wiesner, U. *Chem. Soc. Rev.* **2006**, *35*, 1028-1042.

[3] Piao, Y.; Burns, A.; Kim, J.; Wiesner, U.; Hyeon, T. *Adv. Funct. Mater.* **2008**, *18*, 3745-3758.

[4] Guerrero-Martínez, A.; Pérez-Juste, J.; Liz-Marzán, L. M. *Adv. Mater.* **2010**, *22*, 1182-1195.

[5] He, Q.; Shi, J. *Journal of Materials Chemistry* **2011**, *21*, 5845-5855.

[6] Li, Z.; Barnes, J. C.; Bosoy, A.; Stoddart, J. F.; Zink, J. I. *Chemical Society Reviews* **2012**, *41*, 2590-2605.

[7] Kresge, C. T.; Leonowicz, M. E.; Roth, W. J.; Vartuli, J. C.; Beck, J. S. *Nature* **1992**, *359*, 710-712.

[8] Bass, J. D.; Solovyov, A.; Pascall, A. J.; Katz, A. *J. Am. Chem. Soc.* **2006**, *128*, 3737-3747.

[9] Zhelev, Z.; Ohba, H.; Bakalova, R. *J. Am. Chem. Soc.* **2006**, *128*, 6324-6325.

[10] Lu, J.; Liong, M.; Zink, J. I.; Tamanoi, F. *Small* **2007**, *3*, 1341-1346.

[11] Sharma, K. K.; Asefa, T. *Angew. Chem.* **2007**, *119*, 2937-2940.

[12] Torney, F.; Trewyn, B. G.; Lin, V. S. Y.; Wang, K. *Nat. Nanotechnol.* **2007**, *2*, 295-300.

[13] Sharma, K. K.; Buckley, R. P.; Asefa, T. *Langmuir* **2008**, *24*, 14306-14320.

[14] Zhang, Q.; Lee, I.; Ge, J.; Zaera, F.; Yin, Y. *Adv. Funct. Mater.* **2010**, *20*,

2201-2214.

[15] Yoo, W. C.; Stein, A. *Chem. Mater.* **2011**, *23*, 1761-1767.

[16] Cai, Q.; Luo, Z.-S.; Pang, W.-Q.; Fan, Y.-W.; Chen, X.-H.; Cui, F.-Z. *Chem. Mater.* **2001**, *13*, 258-263.

[17] Sadasivan, S.; Fowler, C. E.; Khushalani, D.; Mann, S. *Angew. Chem. Int. Ed.* **2002**, *41*, 2151-2153.

[18] Büchel, G.; Unger, K. K.; Matsumoto, A.; Tsutsumi, K. *Adv. Mater.* **1998**, *10*, 1036-1038.

[19] Nooney, R. I.; Thirunavukkarasu, D.; Chen, Y.; Josephs, R.; Ostafin, A. E. *Chem. Mater.* **2002**, *14*, 4721-4728.

[20] Kim, M.-H.; Na, H.-K.; Kim, Y.-K.; Ryoo, S.-R.; Cho, H. S.; Lee, K. E.; Jeon, H.; Ryoo, R.; Min, D.-H. *ACS Nano* **2011**, *5*, 3568-3576.

[21] Beck, J. S.; Vartuli, J. C.; Roth, W. J.; Leonowicz, M. E.; Kresge, C. T.; Schmitt, K. D.; Chu, C. T. W.; Olson, D. H.; Sheppard, E. W. *J. Am. Chem. Soc.* **1992**, *114*, 10834-10843.

[22] Larsen, G.; Lotero, E.; Marquez, M. *Chem. Mater.* **2000**, *12*, 1513-1515.

[23] Sayari, A.; Liu, P.; Kruk, M.; Jaroniec, M. *Chem. Mater.* **1997**, *9*, 2499-2506.

[24] Zhao, D.; Feng, J.; Huo, Q.; Melosh, N.; Fredrickson, G. H.; Chmelka, B. F.; Stucky, G. D. *Science* **1998**, *279*, 548-552.

[25] Huo, Q.; Leon, R.; Petroff, P. M.; Stucky, G. D. *Science* **1995**, *268*, 1324-1327.

[26] Boissière, C.; Martines, M. A. U.; Tokumoto, M.; Larbot, A.; Prouzet, E.

Chem. Mater. **2002**, *15*, 509-515.

[27] Li, X.; John, V. T.; Zhan, J.; He, G.; He, J.; Spinu, L. *Langmuir* **2011**, *27*, 6252-6259.

[28] Pan, W.; Ye, J.; Ning, G.; Lin, Y.; Wang, J. *Mater. Res. Bull.* **2009**, *44*, 280-283.

[29] Zhang, H.; Li, Z.; Xu, P.; Wu, R.; Jiao, Z. *Chem. Commun.* **2010**, *46*, 6783-6785.

[30] Polshettiwar, V.; Cha, D.; Zhang, X.; Basset, J. M. *Angew. Chem. Int. Ed.* **2010**, *49*, 9652-9656.

[31] Polshettiwar, V.; Thivolle-Cazat, J.; Taoufik, M.; Stoffelbach, F.; Norsic, S.; Basset, J.-M. *Angew. Chem. Int. Ed.* **2011**, *50*, 2747-2751.

[32] Smith, E. L. *J. Phys. Chem.* **1931**, *36*, 1401-1418.

[33] Wellman, V. E.; Tartar, H. V. *J. Phys. Chem.* **1929**, *34*, 379-409.

[34] Newman, F. R. *J. Phys. Chem.* **1913**, *18*, 34-54.

[35] Winsor, P. A. *Trans. Faraday Soc.* **1948**, *44*, 376-398.

[36] Schwuger, M.-J.; Stickdorn, K.; Schomaecker, R. *Chem. Rev.* **1995**, *95*, 849-864.

[37] Nagarajan, R.; Ruckenstein, E. *Langmuir* **2000**, *16*, 6400-6415.

[38] Kahlweit, M.; Strey, R.; Busse, G. *J. Phys. Chem.* **1990**, *94*, 3881-3894.

[39] Kahlweit, M.; Strey, R.; Firman, P. *J. Phys. Chem.* **1986**, *90*, 671-677.

[40] Kegel, W. K.; Lekkerkerker, H. N. W. *Colloids Surf., A* **1993**, *76*, 241-248.

[41] Monnier, A.; Schüth, F.; Huo, Q.; Kumar, D.; Margolese, D.; Maxwell, R.

S.; Stucky, G. D.; Krishnamurty, M.; Petroff, P.; Firouzi, A.; Janicke, M.; Chmelka, B. F. *Science* **1993**, *261*, 1299-1303.

[42] Kabalnov, A.; Wennerström, H. *Langmuir* **1996**, *12*, 276-292.

[43] Hazlett, R. D.; Schechter, R. S. *Colloids Surf.* **1988**, *29*, 53-69.

Chapter 3

Silica Mesostructures Synthesized on the Basis of the Phase behavior of the Pseudoternary System

3.1 Introduction

Since the introduction of MCM-41, mesoporous silica materials that have large surface areas, pore volumes, and facile surface modification have been widely used for various applications, such as catalyst support, drug delivery, adsorption, separation, electrodes, and as hard templates for structure direction.[1-7] Initially, only mesoporous silica materials in the bulk cluster form were synthesized; subsequently, mesoporous silica nanoparticles were produced for many applications that required colloidal dispersibility.[8-10] Because the particle and pore sizes of the silica nanoparticles affect their physical, chemical, and optical properties, it is very important to control the particle size and morphology of the silica nanoparticles; thus many research groups have investigated methods to achieve this.[10-12]

Recently, mesoporous silica nanoparticles with radial wrinkle structures were introduced almost simultaneously by several groups; wrinkled silica nanoparticles (WSNs) have attracted much attention for their high accessibility to guest materials and large surface area due to their open pore structure.[13-22] In Chapter 2, we suggested a synthetic mechanism for WSNs based on emulsion formation theories and established a method to tune the

inter-wrinkle distance using the phase behaviors of emulsion systems; however, we were unable to control the particle sizes and external morphologies. There has been one report regarding size control of WSNs but the range of controllable particle sizes was very narrow, and size control caused undesirable changes in the emulsion structure and inter-wrinkle distance of the WSNs.[14]

Water-oil-surfactant ternary systems have various phase behaviors, such as a thermodynamically stable microemulsion phase or multi-phase systems containing a microemulsion layer, which depend on the chemical composition or component ratio. In particular, in the case of the multi-phase system that emerges at low surfactant concentrations related to the amount of the two immiscible solvents, the visible bulk-phase behavior corresponds with the molecular behavior and substructure of the microemulsion layer. Accordingly, the structure of the emulsion can be easily identified and tuned. These characteristics have been systematically investigated and established by many researchers including Winsor.[23-25] Winsor classified ternary systems into four types, i.e., type I–IV, according to the numbers and types of phases in the equilibrium state and investigated the structure of the microemulsion layer of each system. Except for the single-phase microemulsion (type IV) with high degrees of freedom, the structure of the microemulsion can be determined via the solvent that separates from the dispersed phase of the microemulsion layer; At equilibrium, superfluous oil separates from the oil-in-water microemulsion in type I, superfluous water separates from the water-in-oil microemulsion in

type II, and both superfluous oil and water separate from the bicontinuous microemulsion in type III. These phase behaviors can be readily controlled via the type of surfactant or cosurfactant and component ratio of the compositions. Because of the variety and ease of control, many studies performed by a variety of researchers have involved the use of the substructures of microemulsions as templates.[26-29] However, most research did not thoroughly survey the phase behavior of the emulsion systems and were limited to investigations of the synthetic method without significant consideration of the relationships among the variables.

In this study, we investigated the global phase behavior of the emulsion system that was used to synthesize wrinkled silica mesostructures (WSMs), and surveyed the relationship between the phase of the emulsions and morphology of the synthesized WSMs. On the basis of this relationship, we established a method to control the internal and external morphology of WSMs. In addition, we studied the effects of the type and concentration of catalyst used in the reaction, thereby controlling the diameter of the spherical WSNs in the range of 50–500 nm. Finally, we produced radially branched WSNs and shuttlecock-shaped Janus silica nanoparticles using the gradual seed-growth mechanism to form silica nanoparticles in the emulsion system.

3.2 Experimental Section

Materials.

Cetyltrimethylammonium bromide (CTAB) was purchased from Aldrich and tetraethylorhtosilicate (TEOS) was purchased from TCI. *n*-Butanol, *n*-pentanol, cyclohexane, sodium hydroxide and urea were purchased from Samchun Pure Chemical. All chemicals were used as received without further purification.

Characterization

Scanning electron microscopy (SEM) and transmission electron microscopy (TEM) were conducted using Hitachi H-4300 and H-7600 instruments, respectively. Nitrogen adsorption-desorption isotherms and pore-size distributions were measured using a Micromeritics ASAP 2020 instrument.

Phase Behavior Analysis of the Pseudoternary System

To simplify the analysis of the multi-component system, we treated a mixture of urea, water, *n*-butanol, cyclohexane, and CTAB as a pseudoternary system and surveyed its phase behavior. For this purpose, some components were paired as pseudocomponents: An aqueous urea solution (0.4 M) was treated as the water component, a mixture of CTAB and *n*-butanol (1:1 w/w) was treated as the surfactant component, and cyclohexane was treated as the oil component. The phase diagram was prepared using a typical progressive dilution method.[24] At first, we prepared 15 compositions of surfactant- water

solutions with weight concentrations in the range of 0–90%. Then, oil was added stepwise into each composition and the points at which the transparency or optical isotropy of the reaction mixture changed were marked on the ternary diagram. The phase diagram was established by connecting the boundary points of the same phase (Fig. 3.1).

Table 3.1. Microemulsion systems used for the synthesis of silica materials with wrinkled structures

Sample	Water:Surfactant:Oil[a]	Type of emulsion system[b]
A	7.5:1.0:1.5	
B	7.5:1.0:3.0	Type II
C	7.5:1.0:4.5	
D	7.5:1.0:7.5	
E	7.5:1.0:10.0	Type III
F	5.0:1.0:10.0	
G	2.0:1.0:10.0	
H	1.5:1.0:10.0	Type I
I	1.0:1.0:10.0	

[a]Weight ratio. Water refers to 0.4 M aqueous urea solution, surfactant refers to a mixture of CTAB/*n*-butanol (1:1 w/w), and oil refers to cyclohexane.
[b]Type I, II, and II refer to the Winsor systems.[25]

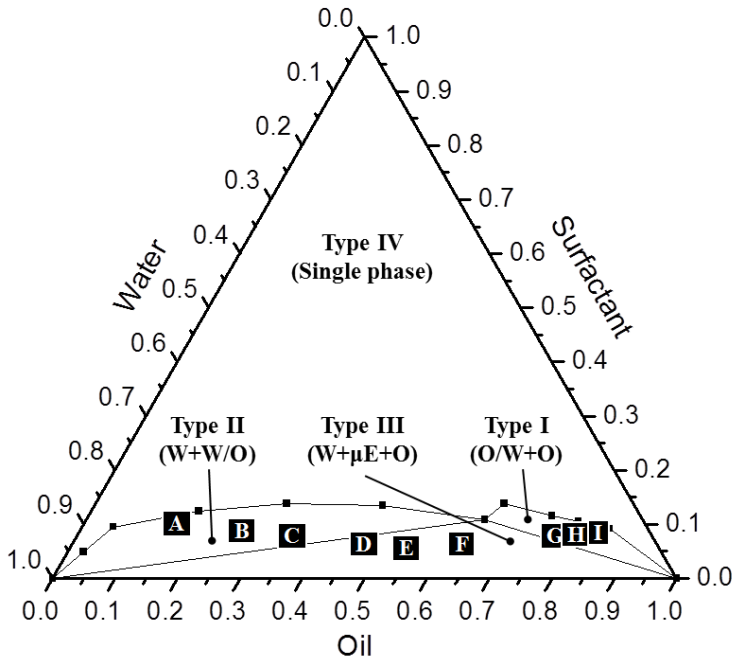

Figure 3.1. Pseudoternary phase diagram of the water/urea + CTAB/*n*-butanol + cyclohexane system at 20 ℃. The concentration of aqueous urea is fixed at 0.4 M, and the mixing ratio of CTAB/*n*-butanol is fixed at 1:1 w/w. The letters on the diagrams refer to the corresponding emulsion compositions in Table 3.1.

Synthesis of Wrinkled Silica Mesostructures on the Basis of Phase Behavior

On the basis of the phase diagram made in a previous survey, we selected some representative reaction mixtures with water-oil-surfactant ratios that corresponded to each type described in the Winsor system. WSMs were synthesized by adding an equivalent of TEOS into each reaction mixture and heating (Table 3.1 and Fig. 3.1). For example, for sample A, 0.5 g of CTAB

and 0.5 g of *n*-butanol were dissolved in 7.5 g of aqueous urea solution (0.4 M). Subsequently, 1.5 g of cyclohexane was added to the solution. With vigorous stirring, 0.5 g of TEOS was added dropwise to the mixed solution. After vigorous stirring for 30 min at room temperature, the reaction mixture was heated to 70 ℃ and held for 20 h. The reaction mixture was centrifuged, washed thrice with acetone and ethanol, and then redispersed in 20 mL of ethanol. To remove the surfactant from the silica nanoparticles, 2 mL of 12 M hydrochloric acid was added and the solution was stirred for 12 h at 70 ℃. The final product was centrifuged and washed thrice with ethanol; subsequently, the solid content was redispersed in 20 mL of ethanol.

Table 3.2. Molar concentrations of acid and base catalysts for the synthesis of wrinkled silica nanoparticles

Sample	Urea (M)	NaOH (mM)	HCl (mM)	Average particle size[a] (nm)
$E_{u0.08}$	0.08	-	-	190
$E_{u0.4}$	0.4	-	-	300
$E_{u2.0}$	2.0	-	-	560
$E_{u0.4n1}$	0.4	1	-	150
$E_{u0.4h1}$	0.4	-	1	80

[a]Measured from the transmission electron micrograph.

Size Control of WSNs via the Catalytic Conditions

In the synthesis described above, the concentration of aqueous urea was varied in the range of 0.08–2.0 M, and specific amounts of sodium hydroxide or hydrochloric acid were added or used solely to determine the effect of the

catalyst components (Table 3.2). For example, for sample $E_{u0.4n1}$, 0.5 g of CTAB and 0.5 g of *n*-butanol were dissolved in 7.5 g of aqueous solution containing of urea (180 mg, 0.4 M) and NaOH (0.3 mg, 10 mM). Subsequently, 10 g of cyclohexane was added to the solution. With vigorous stirring, 0.5 g of TEOS was added dropwise to the mixed solution. After vigorous stirring for 30 min at room temperature, the reaction mixture was heated to 70 ℃, and held for 20 h. The product was purified using the same process mentioned in the above section.

Synthesis of Core-Shell Type WSNs

Amorphous silica nanoparticles (ASNs) and WSNs with wide inter-wrinkle distances synthesized using *n*-pentanol as cosurfactant were prepared using a reported procedure.[13,30] In this synthesis, 0.5 g of CTAB and 0.5 g of *n*-butanol (or isopropanol) were dissolved in 7.5 g of aqueous urea solution (0.4 M). Then 50 mg of the prepared silica nanoparticles (ASNs or WSNs) was added and dispersed in the solution using ultrasonication. Subsequently, 1.5 g of cyclohexane was added to the solution. With vigorous stirring, 0.5 g of TEOS was added dropwise to the mixed solution. After vigorous stirring for 30 min at room temperature, the reaction mixture was heated to 70 ℃, and held for 20 h. The product was purified using the same process mentioned in the above section.

Synthesis of Shuttlecock Shaped WSNs

1.0 g of CTAB and 1.0 g of *n*-pentanol were dissolved in 30 g of aqueous urea solution (0.4 M). Subsequently, 3.0 g of cyclohexane was added to the solution. With vigorous stirring, 1.25 g of TEOS was added dropwise to the mixed solution. After vigorous stirring for 30 min at room temperature, the reaction mixture was heated to 70 ℃, and held for 20 h. The reaction mixture was then cooled to room temperature and 27 g of cyclohexane and 1.25 g of TEOS were added to the reaction mixture. After vigorous stirring for 30 min at room temperature, the reaction mixture was heated to 70 ℃, and held for 20 h. The product was purified using the same process mentioned in the above section.

3.3 Result and Discussion

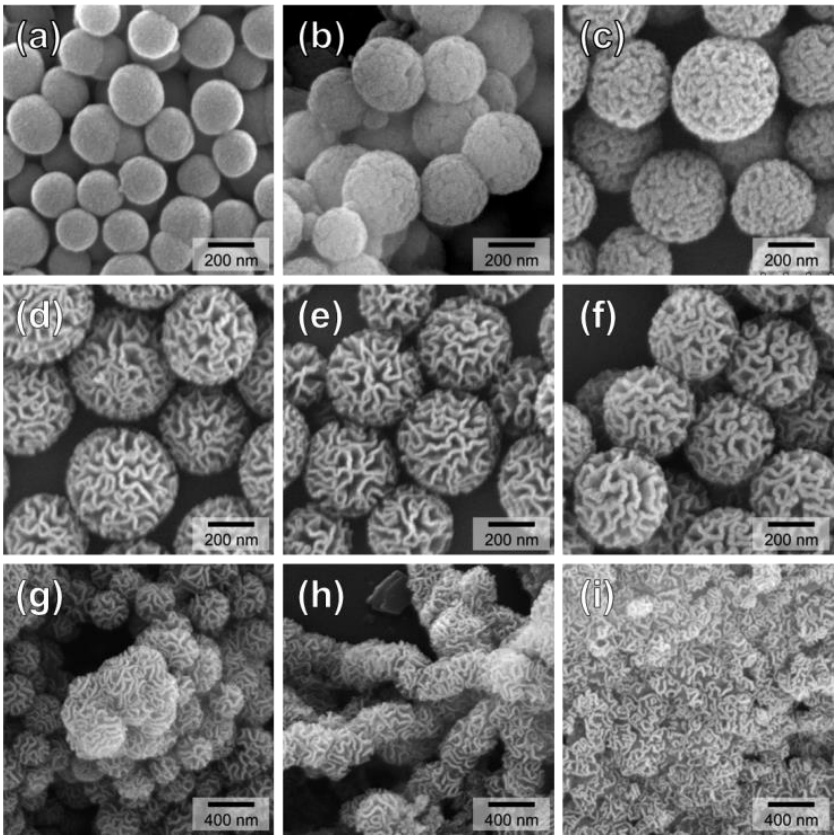

Figure 3.2. (a–i) SEM images of the silica materials synthesized from the corresponding emulsion systems in Table 3.1.

Silica Mesostructures Synthesized on the Basis of the Phase Behavior

The phase behavior of a pseudoternary system that treats a 0.4 M aqueous urea solution as the water component, a mixture of CTAB and *n*-butanol (1:1 w/w) as the surfactant component, and cyclohexane as the oil component is described in Figure 3.1. When the mixture was surfactant-rich area (>15% surfactant), the amount of surfactant was sufficient to dissolve both water and

oil and the emulsion system formed a single-phase microemulsion or anisotropic liquid crystal or lamella phase (Type IV). In contrast, when the mixture was surfactant-poor area (<15% surfactant), a microemulsion layer and extra solvent layer(s) separated from the microemulsion to form multi-phase systems. These systems are labeled as Winsor types I–III according to the relative ratio of water, surfactant, and oil components.

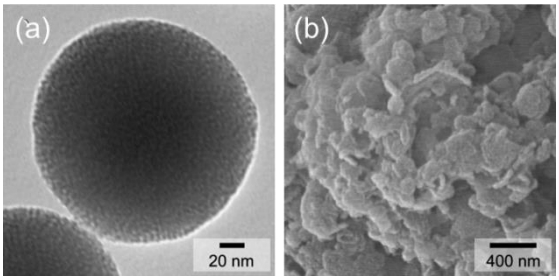

Figure 3.3. (a) TEM image of mesoporous silica nanoparticles synthesized in the type-IV system. The weight ratio of water (with catalyst):surfactant (with cosurfactant):oil in all reaction mixtures was 7.5:1.0:1.0. (b) SEM image of the silica precipitate synthesized in the type-IV system. The weight ratio of water (with catalyst):surfactant (with cosurfactant):oil in all reaction mixtures is 0.25:1.0:10.0.

We synthesized WSMs using various types of emulsion systems in the multi-phase area as structure-directing templates; accordingly, we could control the internal morphology and inter-particle connective structure (Fig. 3.2) as an extension of Chapter 2.[13] The independent mesopores of silica nanoparticles were interconnected and converted to the wrinkled structure depending on the amount of oil in the emulsion system, which started from a

direct micelle (Figs. 3.2a–d and 3.3). This trend was confirmed in Chapter 2.[13] We also confirmed that the WSNs were interconnected and formed an inter-connected bulk gel with wrinkle structures as the amount of water in the emulsion system decreased, beginning from the composition that resulted in the formation of spherical WSNs (Figs. 3.2f–i).

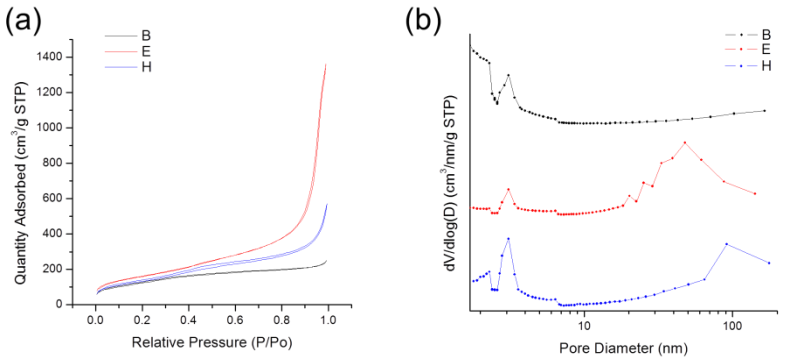

Figure 3.4. (a) N_2 adsorption-desorption isotherms and (b) BJH pore-size distribution plots of representative WSMs synthesized in the emulsion systems shown in Table. 3.1.

The Brunauer–Emmett–Teller (BET) surface areas of WSMs synthesized in different types of systems (i.e., samples B, E, and H in Table 3.1), as measured from the N_2 adsorption-desorption isotherms, were 450.0, 590.6, and 478.8 m^2/g, respectively. The shapes of the N_2 adsorption-desorption isotherms of these mesostructures corresponded with type IV (Fig. 3.4a). For samples E and H, which had distinct wrinkled structures, there were additional large N_2 uptakes and H_3 hysteresis at a relative pressure (P/P_0) near

1.0; these were attributed to the large number of slit-shaped meso/macro-pores.

Sample B contained only poorly developed wrinkles; therefore, there was only a small N_2 uptake at the end of plot and its surface area was smaller than that of sample E. The Barrret–Joyner–Halenda (BJH) pore size distribution plot also showed this difference; Samples E and H contained pores over 20 nm in diameter while sample B did not (Fig. 3.4a). Sample H had a smaller surface area than sample E, which was attributed to its interparticle connectivity and increased size.

The structure of the multiphase emulsion system was determined by the relative concentrations of the water, surfactant, and oil components; its degrees of freedom were defined using Gibbs' phase rule, as follows:[31,32]

$$F= C – P + 2 \quad (1)$$

Where, F is the number of degrees of freedom corresponding to the temperature and pressure, C is the number of independent components, and P is the number of phases of the system. In the case of the system we investigated, the phase behavior was analyzed at a fixed temperature (20 °C) and pressure (1 atm); therefore, the degrees of freedom involved with those two factors were restricted on the supposition that the mixture was a condensed system. If so, the degrees of freedom were defined only by the relative concentration of the three components (water, oil, and surfactant) and could be formulated as follows:

$$F = 3 – P \quad (2)$$

According to the above phase rule, the three-phase area is invariant with zero degrees of freedom, the two-phase area is monovariant with one degree of freedom, and the one-phase area is bivariant with two degrees of freedom. The structural trend of the silica mesostructures synthesized from the pseudoternary mixtures corresponded with the representative points on each type of system in the phase diagram and obeyed this phase rule. In the type-III system, the three-phase area consisted of a bicontinuous microemulsion and an additional water and oil layer; the composition ratio in the microemulsion layer was invariant even if the relative concentration of the total components changed, which resulted in constant substructures of the materials synthesized in this area (Figs. 3.2d–f).

Two-phase areas have one degree of freedom, and the fixed compositions and variable compositions of the system differed with the types of systems. The type-II system had an excess amount of water that is larger than the solubilization capacity of the surfactant; thus, superfluous water separated from the water-in-oil microemulsion layer. Therefore, the composition ratio of the water and surfactant was fixed and only the amount of oil in the microemulsion layer was variable. The amount of oil in the microemulsion affected the volume of the continuous phase and average distances among the dispersed phases. Because the silica-forming reactions began with hydrolysis of TEOS in the dispersed aqueous phase of the emulsion, the continuous oil phase corresponded with the pores of the silica mesostructures formed in the system. Accordingly, the amount of oil defined the volume of the pores. In

our results, the pores of the silica mesostructures synthesized with various amounts of oil in type-II range were interconnected and generated the wrinkled structure as the amount of oil increased (Figs. 3.2a–c); its structural convergence determined the inter-wrinkle distance of the WSNs synthesized in the type-III area (Figs. 3.2d–f).[13]

On the other hand, type-I systems contained excess oil, and superfluous oil separated from the oil-in-water microemulsion layer. Therefore, the composition ratio between oil and surfactant was fixed, and the amount of water in the microemulsion layer was variable. Similar to the effect of the amount of oil in the type-II systems, the amount of water in the microemulsion of the type-I systems influenced the connective morphology of the continuous phase of the microemulsion, and therefore the connectivity of the wrinkled walls of the WSNs. Starting with the three-phase area, as the amount of water decreased, the shared portion of water in the emulsion increased, the WSNs became interconnected, and finally completely interconnected chains resulted in the formation of a gel (Figs. 3.2g–i).

Ultimately, the monophasic microemulsion area had two degrees of freedom, and the composition ratio of the three pseudo-components was variable without any limitations. Because the droplets of microemulsion did not condense in the confined space and diffused freely, silica materials synthesized in this area had independent mesoporous structures (Fig. 3.3a)[13] or irregularly aggregated structures (Fig. 3.3b).

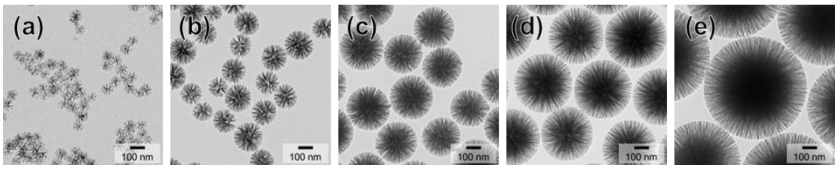

Figure 3.5. TEM images of the wrinkled silica nanoparticles synthesized with various catalytic systems; (a) Urea 0.4 M + HCl 1 mM, (b) urea 0.4 M + NaOH 1 mM, (c) urea 0.08 M, (d) urea 0.4 M, and (e) urea 2.0 M. The weight ratio of water (with catalyst):surfactant(with cosurfactant):oil in all reaction mixtures was 7.5:1.0:10.0.

Size Control of WSNs via the Catalytic Conditions

During the synthesis of silica nanoparticles, the type and concentration of a catalyst affected the diameters of the particles. The catalysts controlled the relative rate of nucleation and growth process of nanoparticles, which determined the rate of hydrolysis of silanes and condensation of silicates. Via control of the catalytic conditions, we adjusted the sizes of spherical WSNs in the range of 50–500 nm (Table 3.2 and Fig. 3.5).

To elucidate the effects of the catalytic conditions during the WSN synthetic process, we observed the pH changes of the water phases of the reactions mixtures using a variety of catalytic conditions during heating at 70 °C (Fig. 3.6). When urea was used as the only catalyst, the pH value initially depended slightly on the concentration of urea, converged to 7 after the temperature of the solutions reached 70 °C, then gradually increased; the pH values at each time period were independent of the urea concentration. The addition of 7.5 μmol of NaOH or HCl to the 0.4 M aqueous urea solution (3.0 mmol of urea in the 7.5 ml of solution) resulted in initial pH values of 10 and

3, respectively; the pH values converged at the equilibrium pH of the urea solutions over time. When the amount of NaOH or HCl added was increased to 75 μmol, the pH values converged toward the pH of the urea solution but did not reach the equilibrium value within the reaction time.

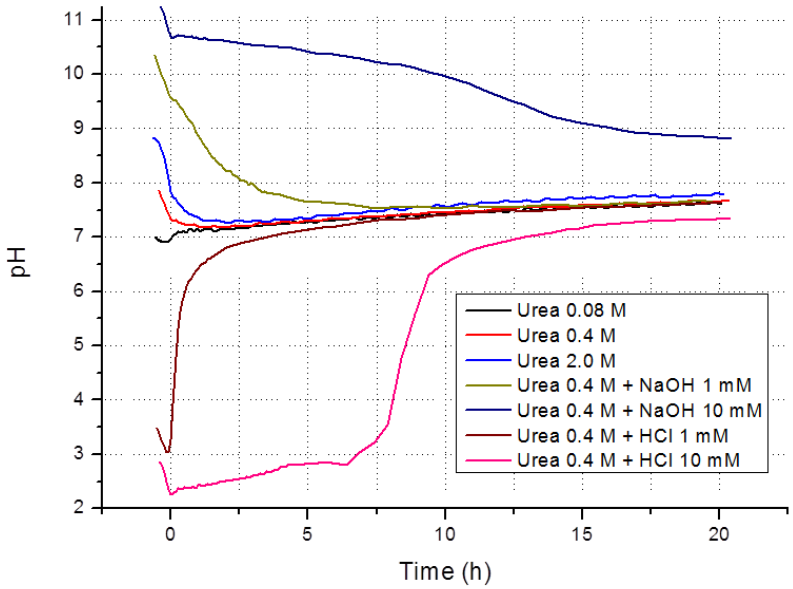

Figure 3.6. Changes in the pH values of the water phases of reaction mixtures during heating at 70 °C. The solutions were heated from room temperature to 70 °C and the time at which the temperatures of the solutions reached 70 °C was defined as the zero-point.

The usual range of pH values of aqueous urea solutions is between 7 and 9.5 depending on the urea concentration. Even though the pH of the pure aqueous urea solution is 7.2 at 10 wt% concentration, practically all commercial grades of urea contain impurities, such as ammonium salts or biuret, which are produced by decomposition of urea and are basic. During

heating to 70 °C, urea decomposes and the products reach equilibrium with ammonium carbonate, resulting in a mildly basic solution. The pH of the reaction mixture initially converged to 7, and then increased continuously because the amount of decomposition products increased during the reaction. Because the decomposition products were volatile and partially soluble, the pH values of reaction mixtures with different urea concentrations were almost equivalent at the same reaction times. The addition of 7.5 μmol of HCl or NaOH to 7.5 mL of 0.4 M aqueous urea solution initially resulted in solutions that were strongly acidic (pH 3) or basic (pH 10), respectively; the pH values of the solutions then converged to that of ammonium carbonate. Increasing the concentration of added HCl of NaOH by ten times prevented complete convergence of the pH values; thus, the amount of HCl or NaOH likely exceeded the amount of ionized ammonium carbonate in the reaction mixture.

We compared WSNs synthesized by adding cyclohexane and TEOS to the above-mentioned conditions. In contrast to WSNs synthesized with only a urea catalyst, increasing the concentration of urea increased the average sizes of the synthesized particles (Figs. 3.5c–e). The effect of the addition of NaOH or HCl to the urea solution was also investigated: As more acid or base was added, the pH value deviated more from 7 and smaller particles formed. When only NaOH was used as a catalyst, smaller particles with random cross-section, i.e., not radial structures, were synthesized as compared to those synthesized when urea was added to the same concentration of NaOH solution.

On the other hand, when only HCl was used as a catalyst, irregular aggregates were formed instead of particles (Fig. 3.7).

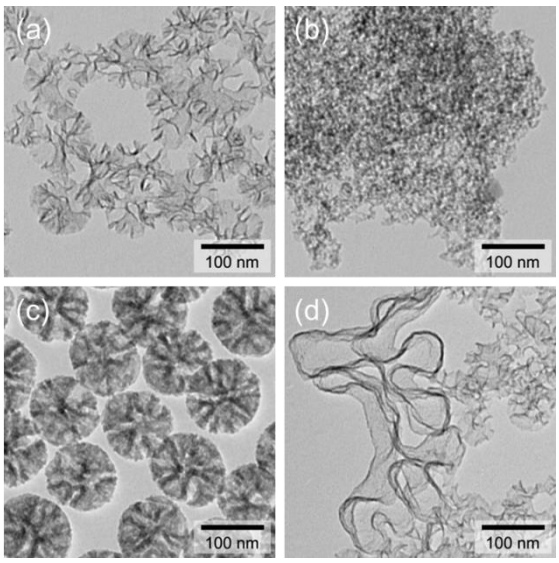

Figure 3.7. TEM images of the wrinkled silica nanoparticles synthesized with various catalytic systems: (a) Urea 0.4 M + NaOH 10 mM, (b) urea 0.4 M + HCl 10 mM, (c) NaOH 1 mM, and (d) NaOH 10 mM. The weight ratio of water (with catalyst):surfactant (with cosurfactant):oil in all reaction mixtures was 7.5:1.0:10.0.

During the synthesis of WSNs, urea initially maintained the neutral pH of reaction mixture and restricted it to a gradual and slow increase. Therefore, the rate of nucleation was regulated and the particle grew gradually. We confirmed this via the radial cross-sections of WSNs. Even with increasing concentration of urea, the pH of the reaction mixtures rarely changed and there was no local rate change during hydrolysis and condensation. However, the number of counter-ions that reduced the repulsive forces among the

clusters that consisted of ionized silicate and cationic surfactant may have increased. Consequently, more clusters gathered in certain spaces and particle growth was promoted, which increased the average particle size of the WSNs.[33]

The addition of NaOH or HCl to the reaction mixture with urea, increased or decreased the initial pH of the solution, respectively, which increased the rate of hydrolysis and nucleation. Then, the pH values of the solutions converged to that of the decomposition products of urea and the same particle-growth process occurred. However, when the amount of NaOH or HCl added exceeded the neutralizing capacity of urea, fast reaction rates were maintained during all the reaction steps and the particles did not grow gradually. Accordingly, the silica nanoparticles with random cross-sections were not radial and gelated structures (i.e., interconnected) were produced. When only NaOH was used as a catalyst, the cross-sections of the synthesized particles were also irregular, and when only HCl was used, the products aggregated without any mesostructures (Fig. 3.7).

Interconnected WSMs synthesized using a type–I systems were also affected by the catalytic conditions. In this system, as the basicity of the reaction mixtures increased, the connectivity of the spherical subunits of the synthesized mesostructures increased (Fig. 3.8). Accordingly, the type–I system had restricted degrees of freedom of the water phase and the synthesis proceeded such that the seeds were contiguous. Thus, the connectivity among the seeds increased as the reaction rate increased.

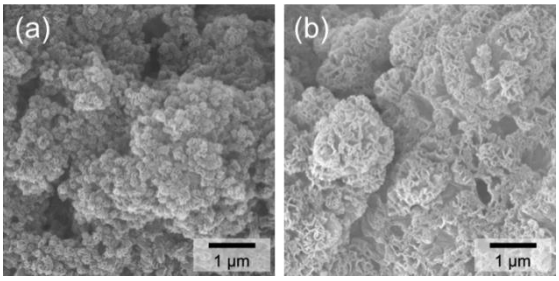

Figure 3.8. SEM images of the wrinkled silica materials synthesized with different catalytic systems: (a) NaOH 10 mM and (b) NaOH 100 mM. The weight ratio of water (with catalyst):surfactant (with cosurfactant):oil in all reaction mixtures was 1.5:1.0:10.0.

Core-Shell Type WSNs

We produced silica nanoparticles with various cross-sectional structures by adding silica nanoparticles with various structures to the reaction mixture of the WSNs (Fig. 3.9). Radially wrinkled silica formed on the surfaces of the core silica nanoparticles. When spherical silica nanoparticles were used as cores, the wrinkled structures formed vertically over the spherical surface; in contrast, when WSNs with wide inter-wrinkle distance were used as cores, the branched wrinkle structures resulted in new wrinkles spreading out over the wrinkled surfaces of the core particles. We controlled the morphology of the secondary wrinkles by changing the cosurfactant used in the second reaction. Apparently, composites with wide and narrow wrinkles can be applied as vehicles for drug delivery with a controlled release rate.

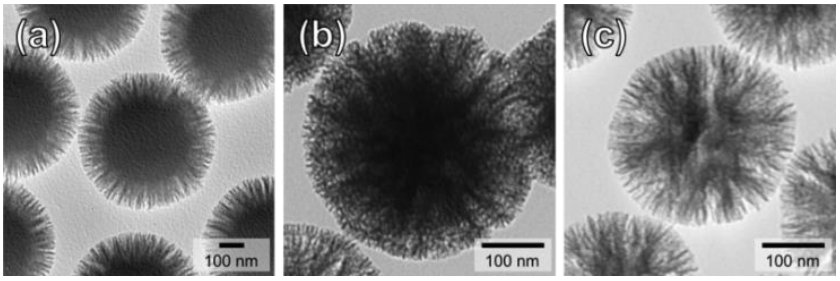

Figure 3.9. TEM images of core-shell type wrinkled silica nanoparticles: (a) $aSiO_2@wSiO_2$, (b) $wSiO_2@wSiO_2$ (cosurfactant: *n*-pentanol → isopropanol), (c) $wSiO_2@wSiO_2$ (cosurfactant: *n*-pentanol → *n*-butanol).

According to Bancroft's rule, components that have higher affinity with the surfactant become the continuous phases and those with lower affinity become the dispersed phases.[34,35] Because the microemulsion layer of the reaction mixtures had a higher affinity with surfactant than the solid particles and expelled solvents, the structure of the macroemulsion formed by stirring consisted of silica nanoparticles and superfluous solvents as the dispersed phases and a microemulsion layer as the continuous phase. Then, secondary WSMs formed in the microemulsion layer and new silica wrinkles grew on the surfaces of the core particles. This process corresponded with the previous radial growth mechanism of WSNs. In the early stage of WSN synthesis, silica seeds were dispersed in the macroemulsion and became contiguous with the microemulsion layer. The radial wrinkled structure was formed by repetitive growth of the wrinkled silica layers around silica seeds. To expand the applicability of the radial growth process, we synthesized a novel silica nanoparticle with a shuttlecock shape via a one-pot synthetic

method (Fig. 3.10). As is well-known, in emulsions with certain compositions, nanoparticles act as surfactants and form supermiclles by self-assembly.[36] Using this supermicelle of spherical silica nanoparticles as a core and generating wrinkled silica on its surface, we formed particles with the expected structures after redispersion (Fig. 3.11). Modification of the surfaces of the head and tail parts of this particle with different ligands is expected to enable this particle to be used as a sort of Janus particle in various applications, such as tandem catalysis, drug delivery, and water-repellent textiles.

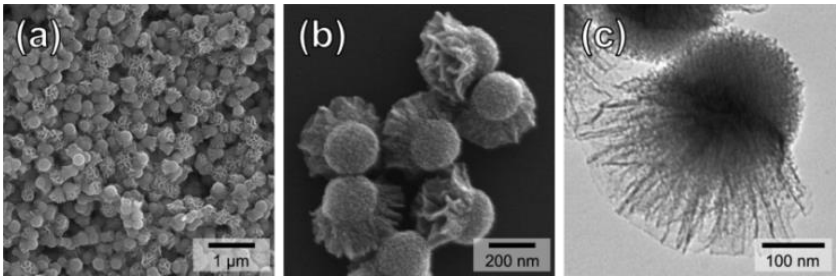

Figure 3.10. (a,b) SEM and (c) TEM images of the shuttlecock shaped nanoparticles.

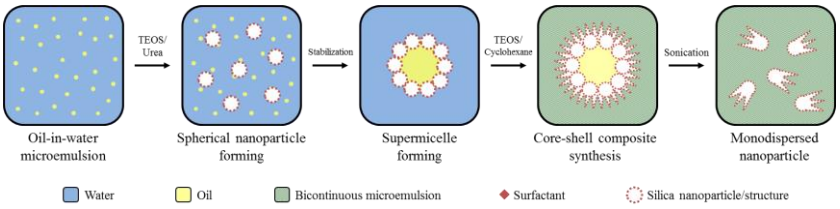

Figure 3.11. Schematic illustration of the formation mechanism of the silica nanoparticle with a shuttlecock shape.

3.4 Conclusion

We investigated the relationship between the emulsion system and morphology of silica mesostructures synthesized in the emulsion as templates via analysis of the phase behavior of a pseudoternary system in which the WSMs formed. On the basis of this study, we established a system to control the internal and external morphology of the WSMs. Also, by controlling the catalytic conditions, we adjusted the sizes of WSNs and connectivity of the interconnected WSMs. Finally, using a radial growth mechanism of WSNs, we synthesized a variety of WSNs with cross-sectional structures and novel shuttlecock-shaped silica nanoparticles.

We foresee that these wrinkled silica mesostructures with tunable substructures, connectivity, and particle sizes will be useful for a variety of applications including drug delivery, adsorption, filtration, catalytic support, and electrodes.

3.5 References

[1] Slowing, I. I.; Trewyn, B. G.; Giri, S.; Lin, V. Y. *Adv. Funct. Mater.* **2007**, *17*, 1225-1236.

[2] Wang, S.; Li, H. *Microporous Mesoporous Mater.* **2006**, *97*, 21-26.

[3] Xi, J.; Qiu, X.; Ma, X.; Cui, M.; Yang, J.; Tang, X.; Zhu, W.; Chen, L. *Solid State Ionics* **2005**, *176*, 1249-1260.

[4] Yang, H.; Shi, Q.; Liu, X.; Xie, S.; Jiang, D.; Zhang, F.; Yu, C.; Tu, B.; Zhao, D. *Chem. Commun.* **2002**, *0*, 2842-2843.

[5] Mercier, L.; Pinnavaia, T. J. *Environ. Sci. Technol.* **1998**, *32*, 2749-2754.

[6] Maschmeyer, T.; Rey, F.; Sankar, G.; Thomas, J. M. *Nature* **1995**, *378*, 159-162.

[7] Kresge, C. T.; Leonowicz, M. E.; Roth, W. J.; Vartuli, J. C.; Beck, J. S. *Nature* **1992**, *359*, 710-712.

[8] Lai, C.-Y.; Trewyn, B. G.; Jeftinija, D. M.; Jeftinija, K.; Xu, S.; Jeftinija, S.; Lin, V. S. Y. *J. Am. Chem. Soc.* **2003**, *125*, 4451-4459.

[9] Sadasivan, S.; Fowler, C. E.; Khushalani, D.; Mann, S. *Angew. Chem. Int. Ed.* **2002**, *41*, 2151-2153.

[10] Nooney, R. I.; Thirunavukkarasu, D.; Chen, Y.; Josephs, R.; Ostafin, A. E. *Chem. Mater.* **2002**, *14*, 4721-4728.

[11] Nandiyanto, A. B. D.; Kim, S.-G.; Iskandar, F.; Okuyama, K. *Microporous Mesoporous Mater.* **2009**, *120*, 447-453.

[12] Vertegel, A. A.; Siegel, R. W.; Dordick, J. S. *Langmuir* **2004**, *20*, 6800-6807.

[13] Moon, D. S.; Lee, J. K. *Langmuir* **2012**, *28*, 12341-12347.

[14] Gai, S.; Yang, P.; Wang, L.; Li, C.; Zhang, M.; Jun, L. *Dalton Trans.* **2012**, *41*, 4511-4516.

[15] Fihri, A.; Cha, D.; Bouhrara, M.; Almana, N.; Polshettiwar, V. *ChemSusChem* **2012**, *5*, 85-89.

[16] Polshettiwar, V.; Thivolle-Cazat, J.; Taoufik, M.; Stoffelbach, F.; Norsic, S.; Basset, J.-M. *Angew. Chem. Int. Ed.* **2011**, *50*, 2747-2751.

[17] Gai, S.; Yang, P.; Ma, P. a.; Wang, D.; Li, C.; Li, X.; Niu, N.; Lin, J. *J. Mater. Chem.* **2011**, *21*, 16420-16426.

[18] Zhang, H.; Li, Z.; Xu, P.; Wu, R.; Jiao, Z. *Chem. Commun.* **2010**, *46*, 6783-6785.

[19] Polshettiwar, V.; Cha, D.; Zhang, X.; Basset, J. M. *Angew. Chem. Int. Ed.* **2010**, *49*, 9652-9656.

[20] Pan, W.; Ye, J.; Ning, G.; Lin, Y.; Wang, J. *Mater. Res. Bull.* **2009**, *44*, 280-283.

[21] Shen, D.; Yang, J.; Li, X.; Zhou, L.; Zhang, R.; Li, W.; Chen, L.; Wang, R.; Zhang, F.; Zhao, D. *Nano Lett.* **2014**, *14*, 923-932.

[22] Du, X.; Shi, B.; Liang, J.; Bi, J.; Dai, S.; Qiao, S. Z. *Adv. Mater.* **2013**, *25*, 5981-5985.

[23] Wennerstro¨m, H.; So¨derman, O.; Olsson, U.; Lindman, B. *Colloids Surf., A* **1997**, *123–124*, 13-26.

[24] Ayyub, P.; Maitra, A.; Shah, D. O. *J. Chem. Soc., Faraday Trans.* **1993**, *89*, 3585-3589.

[25] Winsor, P. A. *Trans. Faraday Soc.* **1948**, *44*, 376-398.

[26] Yang, W.; Li, B. *Nanoscale* **2014**, *6*, 2292-2298.

[27] Lin, Y.-S.; Wu, S.-H.; Tseng, C.-T.; Hung, Y.; Chang, C.; Mou, C.-Y. *Chem. Commun.* **2009**, 3542-3544.

[28] Stubenrauch, C.; Wielpütz, T.; Sottmann, T.; Roychowdhury, C.; DiSalvo, F. J. *Colloids Surf., A* **2008**, *317*, 328-338.

[29] Rees, G. D.; Evans-Gowing, R.; Hammond, S. J.; Robinson, B. H. *Langmuir* **1999**, *15*, 1993-2002.

[30] Stöber, W.; Fink, A.; Bohn, E. *J. Colloid Interface Sci.* **1968**, *26*, 62-69.

[31] Cistola, D. P.; Hamilton, J. A.; Jackson, D.; Small, D. M. *Biochemistry* **1988**, *27*, 1881-1888.

[32] Smith, D. H.; Wang, Y.-H. C. *J. Phys. Chem.* **1994**, *98*, 7214-7218.

[33] Knecht, M. R.; Sewell, S. L.; Wright, D. W. *Langmuir* **2005**, *21*, 2058-2061.

[34] Bancroft, W. D. *J. Phys. Chem.* **1912**, *17*, 501-519.

[35] Binks, B. P. *Langmuir* **1993**, *9*, 25-28.

[36] Bollhorst, T.; Grieb, T.; Rosenauer, A.; Fuller, G.; Maas, M.; Rezwan, K. *Chem. Mater.* **2013**, *25*, 3464-3471.

Appendix

Synthesis and Application of Fe_3O_4@wSiO_2 Nanocomposite as a Biosensor

1. Introduction

As discussed in main chapters, wrinkles silica mesostructures (WSM) have large surface area and good accessibility because of its radial wrinkle structures. And the synthetic method is quiet easy and conducted in mild conditions. In addition, it is possible that the WSMs can be coated on other nanoparticles including silica nanoparticles as the shell. In this appendix, the core-shell type nanocomposite of WSM on the magnetite nanoparticle is synthesized using these properties of WSMs. And simple cell uptake test and bioimaging test are conducted to show the potential of WSMs in drug delivery applications.

2. Experimental Section

Chemicals and Instrumentation

97% Iron (III) chloride hexahydrate, polyacrylic acid (PAA, Mw: 1800) were purchased from Sigma-aldrich, rhodamine B isothiocyanate (RITC), cetylpyridinium bromide (CPB) were purchased from Aldrich, (3-trimethoxysilylpropyl)diethylenetriamine (DETAS), triethylorhtosilicate (TEOS) were purchased from TCI. 98.5% Sodium acetate trihydrate, acetic acid, urea, cyclohexane, ethylene glycol, and *n*-butanol were purchased from Samchun Pure Chemical. All chemicals were used as received without further purification.

Analyses with scanning electron microscopy (SEM) and transmission electron microscopy (TEM) were conducted using Hitachi H-4300 and H-7600 instruments, respectively.

Synthesis of Fe_3O_4 Magnetic Nanoparticles

Fe_3O_4 magnetic nanoparticle with average 100 nm diameters was synthesized via previously reported method.[1,2] 27 g of $FeCl_3 \cdot 6H_2O$ was solvated in 750 ml of ethylene glycol and 100 g of $NaAc \cdot 3H_2O$ and 100g of D.I. water are solvated in 750 ml of ethylene glycol. After the mixing of two totally solvated solutions, the mixture was stirred for 300 rpm with mechanical stirrer and the heated up to 70 ℃. After maintaining for 1 hour in that temperature, the mixture turns into suspension of red-brown. Then the reaction mixture was refluxed for 24 hours, the temperature of reaction

mixture was maintained 160 ℃. After the reaction was terminated, formed black nanoparticles were purified with centrifugations with 4000 rpm for 10 minutes then washed with ethanol three times. The purified nanoparticles were used as dispersed in D.I. water. Magnetic nanoparticle with 50 nm diameter was synthesized via same reaction procedure but the amount of $FeCl_3 \cdot 6H_2O$ was reduced to 24 g.

Surface Modification of Fe_3O_4 Magnetic Nanoparticles with PAA

3 g of PAA (Mw: 1800) was solvated in 100 ml of each aqueous solution that 1 g of Fe_3O_4 magnetite nanoparticle was dispersed in, then the solution was ultrasonicated for 1 hour and stirred for 6 hours at R.T. After the reaction was completed the PAA coated nanoparticle was precipitated with centrifugation of 8000 rpm for 10 mins then redispersed and used in 10 ml of 2.5% $NH_4OH_{(aq)}$.

Synthesis of Fe_3O_4@aSiO_2

10 ml of aqueous colloidal solution contains Fe_3O_4 nanoparticle whose surface modified with PAA was added into 90 ml of ethanol and the mixture was stirred for 30 min.[3-5] Then 0.1 ml of TEOS was added into the mixture and reacted for 12 hour at R.T. After the reaction was completed, reacted nanoparticles were purified with centrifugations with 15000 rpm for 10 minutes then washed with water three times. And the nanoparticles were redispersed in water for 5 mg/ml concentration.

Synthesis of Fe_3O_4@wSiO_2 Nanocomposite.[6]

1.0 g of CPB and 0.3 g of urea were added into 15 ml of aqueous colloidal solution that 75 mg of Fe_3O_4@aSiO_2 nanoparticle was dispersed in. To this solution, 15 ml of cyclohexane, 0.55 ml of *n*-butanol and 0.5 ml of TEOS were added and the mixture was stirred for 30 minutes at R.T. The white cloudy emulsion made by stirring was heated up to 70 ℃ and reacted for 16 hours. The reaction mixture was centrifuged, washed thrice with acetone and ethanol, and then redispersed in 50 mL of ethanol. To remove the surfactant from the silica nanoparticles, 5 mL of acetic acid was added and the solution was stirred for 12 hours at 70 ℃. The final product was centrifuged and washed thrice with ethanol; subsequently, the solid content was redispersed in 20 mL of ethanol.

RITC Labeling of Fe_3O_4@wSiO_2 Nanocomposite

After addition of 50 mg of DETAS into 10 ml of 5 mg/ml Fe_3O_4@wSiO_2 ethanol solution, the reaction mixture was stirred for 12 hours at R.T. Then the reaction mixture was centrifuged, washed thrice with ethanol, and then redispersed in 10 mL of ethanol. In this solution, 10 mg of RITC was added and the solution was stirred for 12 hours at R.T. The RITC-labeled nanoparticle was centrifuged and washed thrice with water and ethanol; subsequently, the solid content was redispersed in 10 mL of water.

Cell Uptake Test of RITC-labeled Fe_3O_4@wSiO_2 Nanocomposite

Aqueous colloidal solutions of RITC-labeled Fe_3O_4@wSiO_2 nanocomposites containing 50 nm and 100 nm Fe_3O_4 nanoparticles as cores were added into each HeLa cell line and consequently the concentration of the nanoparticles in the mixtures became 150 μg/ml. Then the cell uptake was performed for 15 minutes. And the same cell uptake test was conducted with neodymium magnets which were placed under the solutions to show the effect of a magnetic field on the magnetic nanocomposite. Then the cell lines were washed thrice with PBS buffer and water to eliminate the nanoparticles which didn't absorbed into the cell. And the cells were analyzed with a fluorescence microscope.

***In-vivo* Bioimaging with RITC-labeled Fe_3O_4 @wSiO_2 Nanocomposite**

Each 150 μg of Fe_3O_4@wSiO_2 nanocomposite with 100 nm core were injected in the body of two rats via tail vein. A neodymium magnet was attached on the chest of one of rats to show the effect of a magnetic field on the magnetic nanocomposite. After 1 hour of incubation, optical imaging with fluorescence was conducted then a certain amount of tissues were collected from heart, liver, and kidney. The collected tissues were analyzed with fluorescence microscope.

3. Result and Discussion

Synthesis of Core-Shell Type Magnetic Nanocomposite

For applications of WSMs as bioimaging material and drug delivery vehicle, we prepared magnetic nanocomposites consist of magnetite nanoparticle as the core and WSM as the shell. Amorphous silica coated Fe_3O_4 nanoparticles were dispersed in the emulsion which used in WSN synthesis and the WSN synthetic reaction was conducted *in-situ*. As a result, we confirmed that the wrinkles silica shell was successfully coated on the Fe_3O_4@aSiO_2 (Fig. A1)

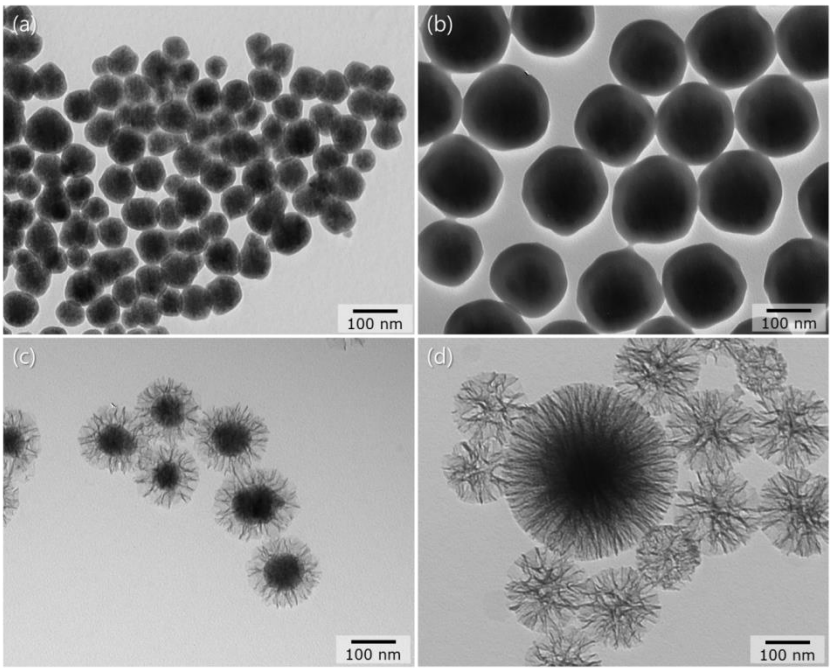

Figure A1. Fe_3O_4@aSiO_2 and Fe_3O_4@wSiO_2 nanocomposites synthesized from Fe_3O_4 core particles with different diameter. Fe_3O_4@aSiO_2 from (a) 50 nm, (b) 100 nm core, and Fe_3O_4@wSiO_2 from (c) 50 nm, (d) 100 nm core.

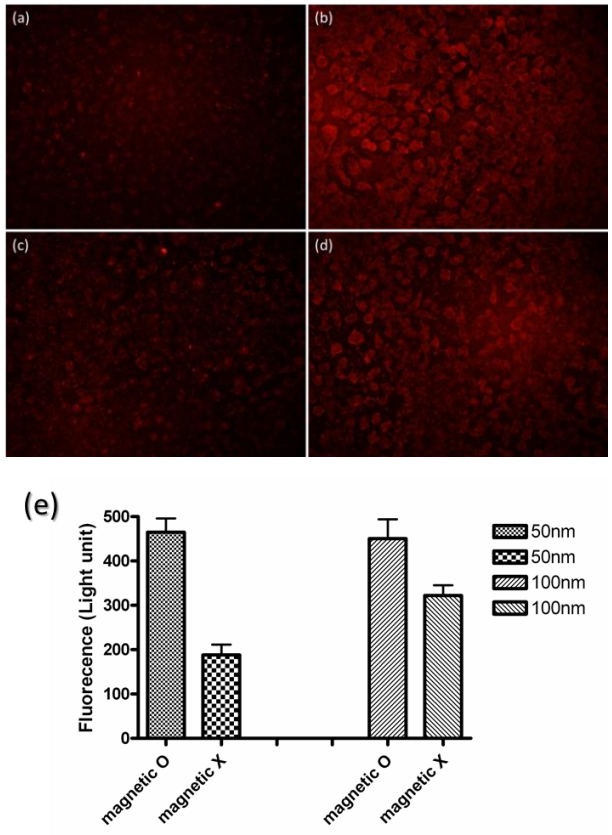

Figure A2. (a-d) Fluorescence microscope images after cell uptake test using nanocomposites from (a,b) 50 nm core (c,d), 100 nm core in the conditions that the magnetic field is (a,c) applied, (b,d) not applied. (e) Quantitative comparison of signals of each image.

Cell Uptake Test

To use the synthesized magnetic nanocomposites as monitoring material, the RITC labeling was conducted. Using these RITC-labeled magnetic nanocomposites, cell uptake test with magnetic field was followed. As a result, we could confirm that the magnetic field affected to the amount of nanocomposites which get into the cytoplasm of the cells (Fig. A2). If the external magnetic field was not applied, very small amount of particles got

into the cells. But when the external magnetic field was applied, lager amount of particle got into the cells. For this result, it seems possible that guided drug delivery with our magnetic nanocomposite by external magnetic field.

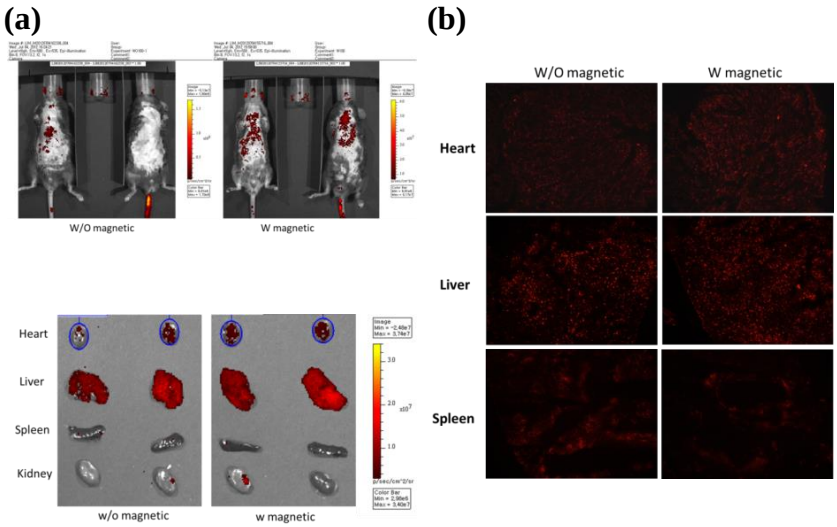

Figure A3. Results of the *In-vivo* bioimaging test. (a) Optical images with fluorescence of rats and collected tissues, (b) fluorescence microscope image of collected tissues.

In-vivo Bioimaging using Fe_3O_4@wSiO_2 Nanocomposite

To confirm the potential of a Fe_3O_4@wSiO_2 nanocomposite as a guided drug delivery supports. The *in-vivo* bioimaging experiments using rats were conducted at first. As a guiding force of nanocomposite, external magnetic field was applied by the neodymium magnet attached on the chest of the rat. As a result, more nanocomposites gathered into the heart of rats that the external magnetic field was applied on those chests. So it is confirmed that the external magnetic field is effective to guide the magnetic nanocomposite to

desired place. But there was limitation of guidance that the most of nanocomposites were accumulated in liver and kidney by the metabolism of body. To solve this problem, It is necessary that the size control and surface modification of nanocomposite to enhance its dispersibility *in-vivo*.

4. Conclusion

Core-shell type wrinkled silica magnetic nanocomposite has both properties of WSNs such as large surface area and good accessibility and magnetic nanoparticles which can be gathered by external magnetic field. So it enhances the possibility of applications in targeted drug delivery and bioimaging. By the *in-vitro* cell uptake tests and *in-vivo* bioimaging experiments, we could find that the guidance of magnetic nanocomposites to desired place was possible with external magnetic field. More study about actual *in-vivo* drug delivery will be discussed after clearing of current several problems such as the accumulation of nanoparticles in liver and kidney.

5. References

[1] Cha, J.; Lee, J. S.; Yoon, S. J.; Kim, Y. K.; Lee, J.-K. *RSC Advances* **2013**, *3*, 3631-3637.

[2] Deng, H.; Li, X.; Peng, Q.; Wang, X.; Chen, J.; Li, Y. *Angew. Chem. Int. Ed.* **2005**, *44*, 2782-2785.

[3] Ó Dálaigh, C.; Corr, S. A.; Gun'ko, Y.; Connon, S. J. *Angew. Chem. Int. Ed.* **2007**, *46*, 4329-4332.

[4] Stöber, W.; Fink, A.; Bohn, E. *J. Colloid Interface Sci.* **1968**, *26*, 62-69.

[5] Deng, Y.; Qi, D.; Deng, C.; Zhang, X.; Zhao, D. *J. Am. Chem. Soc.* **2007**, *130*, 28-29.

[6] Moon, D. S.; Lee, J. K. *Langmuir* **2012**, *28*, 12341-12347.

Korean Abstract

최근 들어 방사형의 주름구조를 갖는 실리카 나노입자가 여러 그룹에 의해 거의 동시다발적으로 소개되었다. 주름구조 실리카 메조구조체는 (wrinkled silica mesostructures, 이하 WSM) 특유의 개방적인 기공구조로 인해 객체 물질들의 높은 접근성과 넓은 표면적을 가지고 있어서 많은 관심을 받았다. 그러나 WSM의 합성에 관한 메커니즘 적인 연구는 아직까지도 충분히 진행된 바가 없다. 이러한 WSM의 형성 메커니즘을 확립하기 위하여 본 논고에서는 WSM의 조절 가능한 합성 경로가 제안되었다.

제 1장에서는 방사형의 주름 구조를 갖는 계층적인 메조기공 구조 실리카 나노입자의 (wrinkled silica nanoparticle, 이하 WSN) 형성 메커니즘에 관한 연구를 수행하였고 WSN의 하위 구조를 조절할 수 있는 합성법을 제안하였다. 우리는 WSN이 Winsor III 유형의 에멀젼계 내부의 복연속상 마이크로에멀젼 층에서 만들어짐을 확인하였다. 물-기름-계면활성제의 혼합비나 조용매의 추가에 따라 결정되는 Winsor III 계의 상거동을 이용하여, 실리카 나노입자의 하부구조를 구형 메조기공 구조로부터 주름 구조에 이르기까지 정밀하게 조절할 수 있었고, 주름들 사이의 간격 또한 용이하게 조절할 수 있었다.

제 2장에서는 화학적 구성성분과 조성비에 따라 다양한 상거동과

하위구조를 갖는 물-기름-계면활성제의 삼원계를 심도 있게 분석하였다. 이러한 하위구조는 다양한 나노구조체의 합성에 있어서 거푸집으로서 사용될 수 있다. 이 연구에서 요소 수용액 - 세틸트리메틸암모늄 브로마이드 및 *n*부탄올 - 시클로헥산으로 구성된 의사삼중계의 상거동이 분석되었다. 그리고 다중상 영역에 있는 의사삼중계의 제한된 자유도를 갖는 마이크로에멀젼 층을 거푸집으로 사용하여 다양한 형상을 갖는 WSM들을 합성하였다. WSN들의 입자크기나 WSM의 연결 경향은 촉매조건을 조절함으로써 결정할 수 있었다. 또한, 에멀젼계 내부에서 일어나는 실리카의 점진적 성장 메커니즘을 이용하여 방사형으로 가지 달린 WSN이나 셔틀콕 형태의 양면 나노입자와 같이 복잡한 형상을 갖는 물질들을 만들 수 있었다.

핵심어: 메조기공체, 실리카, 나노입자, 상거동, 삼원 에멀젼계, Winsor 계, 마이크로에멀젼

학번: 2008-22724